The Berkovići (BIH) ML = 6.0 earthquake sequence of 22 April 2022 – seismological and seismotectonic analyses

Dasović, Iva; Herak, Marijan; Herak, Davorka; Latečki, Helena; Sečanj, Marin; Tomljenović, Bruno; Cvijić-Amulić, Snježana; Stipčević, Josip

Source / Izvornik: **Tectonophysics: The International Journal of Integrated Solid Earth Sciences, 2024, 875**

Journal article, Published version
Rad u časopisu, Objavljena verzija rada (izdavačev PDF)

https://doi.org/10.1016/j.tecto.2024.230253

Permanent link / Trajna poveznica: https://urn.nsk.hr/urn:nbn:hr:169:136405

Tectonophysics 875 (2024) 230253

Contents lists available at ScienceDirect

Tectonophysics

journal homepage: www.elsevier.com/locate/tecto

The Berkovići (BIH) $M_L = 6.0$ earthquake sequence of 22 April 2022 – Seismological and seismotectonic analyses

Iva Dasović [a,*], Marijan Herak [a], Davorka Herak [a,1], Helena Latečki [a], Marin Sečanj [a], Bruno Tomljenović [b], Snježana Cvijić-Amulić [c], Josip Stipčević [a]

[a] Department of Geophysics, Faculty of Science, University of Zagreb, Horvatovac 95, 10000 Zagreb, Croatia
[b] Faculty of Mining, Geology and Petroleum Engineering, University of Zagreb, Pierottijeva 6, 10000 Zagreb, Croatia
[c] Republic Hydrometeorological Institute of Republic of Srpska, Banja Luka, Bosnia and Herzegovina, Put Banja Luka odreda bb, 78000 Banja Luka, P.O. Box: 147, Republic of Srpska, Bosnia and Herzegovina

ARTICLE INFO

Keywords:
Aftershock locations
First-motion polarity focal mechanisms
Earthquake location uncertainty
The External Dinarides
Basal thrust of the Dalmatian unit

ABSTRACT

In the southeast of Bosnia and Herzegovina, the Berkovići earthquake sequence started with the mainshock on 22 April 2022 21:07 UTC at focal depth 22 km with magnitude $M_L = 6.0$ ($M_w = 5.7$). Our preliminary estimation of the mainshock's maximum intensity is VII EMS for Berkovići where 29% of buildings were damaged. We analysed the first nine months of this sequence, 22 April 2022–22 January 2023. The earthquakes were located using a guided grid-search algorithm with source-specific station corrections as a mean of solutions for 54 combinations of velocity models and program control parameters. The analysis of aleatory variation and epistemic uncertainty showed that they are very dependent on the station coverage, especially for focal depth. The event catalogue consists of 7217 earthquakes and can be considered complete for $M_L \geq 1.3$. Focal depths (15–30 km) are considerably larger than average for the Dinarides, but consistent within the zone of mid-crustal events where the earthquakes occurred. Focal mechanisms were determined with the first-motion polarity method for eight earthquakes: five of them, including the mainshock, were due to reverse faulting on faults striking in the Dinaric direction, with the preferred main fault gently dipping to the northeast. However, three events were due to normal faulting, unexpected for this area. We constructed a regional seismotectonic cross-section to delineate a potential seismogenic source of the mainshock, and it suggests that the mainshock occurred on the NE-dipping blind ramp of the basal thrust of the Dalmatian tectonic unit. Moreover, another NE-dipping and blind ramp of this basal thrust could be responsible for the Ston–Slano 1996 earthquake, located to the SW of the Berkovići mainshock hypocentre at the horizontal distance of c. 35 km.

1. Introduction

The southern External Dinarides are seismically moderately to highly active area. The historical seismicity catalogue for this region, e.g. Croatian Earthquake Catalogue (CEC; updated regularly from Herak et al., 1996), includes numerous strong events, the largest of them being the devastating Dubrovnik earthquake of 1667. Moreover, at the far south near Bar, Montenegro, an earthquake $M_L = 6.8$ (CEC; $M_W = 6.9$, International Seismological Centre, 2021) occurred in 1979. However, geometry and properties of the complex fault systems in the area are still not known well enough. These are essential for improvement of seismic hazard assessment in this area, and for advancement of our understanding of seismotectonic and structural relations. Accurate location and characterisation of contemporary seismicity (including very weak earthquakes) is one of the means towards this goal. The Berkovići earthquake sequence occurred a few months after deployment of four broadband seismic stations in an area of about 60 km radius around the mainshock, and several more instrument deployments have followed since (see section 3.1). Furthermore, it is the first earthquake of this size in south of the External Dinarides to be monitored with such a quantity

* Corresponding author.
E-mail addresses: iva.dasovic@gfz.hr (I. Dasović), marijan.herak@gfz.hr (M. Herak), davorka.herak@retired.pmf.hr (D. Herak), helena.latecki@gfz.hr (H. Latečki), marin.secanj@gfz.hr (M. Sečanj), bruno.tomljenovic@rgn.unizg.hr (B. Tomljenović), s.cvijic-amulic@rhmzrs.com (S. Cvijić-Amulić), josip.stipcevic@gfz.hr (J. Stipčević).
[1] Retired.

https://doi.org/10.1016/j.tecto.2024.230253
Received 21 June 2023; Received in revised form 2 February 2024; Accepted 15 February 2024
Available online 17 February 2024

of modern instruments.

The last strong earthquake in the wider Dubrovnik area, as well the southern External Dinarides, was the Ston–Slano (Croatia) earthquake of 5 September 1996. Its local magnitude was $M_L = 6.0$ ($M_W = 6.0$, International Seismological Centre, 2021) and maximum intensity was estimated as I_{max} = VIII Medvedev–Sponheuer–Karnik scale (hereafter MSK; updated from Medvedev et al., 1964 and Medvedev, 1978). This earthquake sequence is well studied with results reported by Markušić et al. (1998), Herak et al. (2010) and Govorčin et al. (2020). However, for this specific area the most interesting is the historical catastrophic earthquake in Dubrovnik (Croatia) on 6 April 1667. Its epicentral intensity was estimated at I_0 = IX MSK and the mainshock was felt about 400 km away – detail description can be found in, e.g. Albini (2015), Albini and Rovida (2016) and Herak et al. (2017). Since the Great Dubrovnik earthquake several strong events occurred in this area, such as the ones in Ston (Croatia) 1850 I_{max} = VIII–IX EMS (Herak et al., 2023; European Macroseismic Scale – EMS, Grünthal, 1998), and M_L = 6.1 close to Ljubinje (Bosnia and Herzegovina) in 1927, which still lacks a detailed study.

The studied earthquake sequence began on 22 April 2022 with the mainshock of $M_L = 6.0$ ($M_w = 5.7$) with the epicentre near the village of Berkovići in the southeastern Bosnia and Herzegovina. This is the epicentral area of only moderate instrumentally well-recorded seismicity in the last ≈75 years, but where significant historical events are known to have occurred (e.g. the Ljubinje earthquake of 1927 mentioned above). Moreover, the Berkovići mainshock hypocentre was unexpectedly deep, at 22 km. The amount of damage reported from the epicentral area, the results of the moment-tensor inversions reported by international agencies (see section 3.2) and preliminary InSAR results showing the absence of a significant co-seismic signal (Simone Atzori, Twitter@SimoneAtzori73; *URL*1, 2023) agreed with the obtained depth. Because of its considerable magnitude, uncommon focal depth and the area that is under-researched, this is an interesting and important earthquake that needs to be thoroughly investigated, both seismically and tectonically.

We present results of the detailed analysis of the first nine months of the series, i.e. 22 April 2022–22 January 2023. The earthquakes were located using a guided search algorithm with implemented source-specific station corrections (Herak et al., 2021), and spatial and temporal analyses of the aftershock sequence are reported. Focal mechanisms were estimated with the first-motion polarity method (Herak et al., 2016) and compared with the available solutions obtained by the moment tensor inversion techniques reported by international institutions.

The results of the seismological analyses (e.g. fault plane solutions and spatial distribution of the aftershocks) indicated activation of gently NE-dipping thrust with tectonic transport top to SW. Taking into consideration the depth of the mainshock, this thrust could not be ad hoc linked to any nearby known faults or deformation structures on the surface. Therefore, we constructed a regional geological cross-section to gain a better understanding of the Berkovići earthquake sequence and to delineate potential seismogenic source.

The mainshock epicentral area is a rural, mountainous region of low population density. Our preliminary estimation of the mainshock's maximum intensity is VII EMS for the Municipality of Berkovići where 29% of buildings were damaged. In Stolac, the largest town in the area, a woman lost her life to a rockfall caused by an earthquake and ten people were injured, however, we estimated the intensity as VI–VII EMS. In Ljubinje we estimated the intensity as VI–VII EMS. The damage was reported within about 40 km from the mainshock epicentre, yet damaged buildings were mostly of vulnerability class A–B, and many of them were in relatively poor condition. The average radius of the intensity IV EMS is found to be about 150 km. The greater area affected by the earthquake is a karstic area and buildings are mostly built on a hard rock. More detailed macroseismic analysis is presented in the Appendix.

2. Seismotectonic setting

2.1. Seismicity

The southern External Dinarides is one of the seismically most active areas of the Dinarides. It encompasses three neighbouring countries: Bosnia and Herzegovina, Croatia, and Montenegro. Seismicity of the area where the Berkovići sequence occurred is entirely in Bosnia and Herzegovina. However, because of its vicinity and importance for the southernmost Croatia (the wider Dubrovnik area), it is monitored by several seismic networks, and the recordings are routinely analysed by Croatian seismologists at the Department of Geophysics, Faculty of Science, University of Zagreb. It is thus also covered by the Croatian Earthquake Catalogue (CEC; Herak et al., 1996). In Fig. 1, we show events $M_L \geq 4.5$ for the period 1600–1990 and $M_L \geq 1.0$ with maximum allowed standard error for the epicentre $\sigma_{h,max} \leq 3.0$ km for the period of 1991–2023.

The wider area of Berkovići is among the most active regions of the southern External Dinarides. Most of the seismicity prior to the 2022 sequence is situated to the west of the mainshock epicentre. Since 1600, in the circle of 25 km radius, three earthquakes with local magnitudes $M_L \geq 5.5$ occurred. On 1 August 1907, an earthquake of epicentral intensity I_0 = VII–VIII MCS (Mercalli–Cancani–Sieberg intensity scale) and an estimated macroseismic magnitude $M_m = 5.7$ occurred at the focal depth h = 12 km, 23 km to the west of the Berkovići mainshock. The strongest and the closest event occurred on 14 February 1927 – an earthquake of I_0 = VIII MCS and $M_L = 6.1$ at h = 13 km with epicentre near Ljubinje, 15 km to the southwest of the 2022 mainshock. It caused damage in Ston, 35 km from the epicentre. The last one occurred on 26 November 2019 and was $M_L = 5.5$ ($M_w = 5.4$) at h = 16 km and 21 km to the northwest of the Berkovići mainshock. Four earthquakes $M_L \geq 6.0$ within 50 km radius from Berkovići that occurred since 1600 had epicentres in Croatia, close to the Adriatic coastline. To the southwest of Berkovići, two events had magnitude 6.0: 13 April 1850 near Ston (M_m = 6.0, I_{max} = VIII–IX EMS; Herak et al., 2023), and the Ston–Slano earthquake of 5 September 1996 ($M_L = M_w = 6.0$, I_{max} = VIII MSK, h = 13 km). To the south of Berkovići, other two events occurred in 17th century in the proximity of Dubrovnik: on 28 July 1639 with I_{max} = VIII MCS (estimated magnitude $M_m = 6.2$), and the Great Dubrovnik earthquake on 6 April 1667 of I_{max} = IX MCS and $M_m = 6.9$.

In this region (Fig. 1a), the earthquake hypocentres are mostly located in the upper crust, down to about 20 km. However, events closer to the coastline are shallower, typically above 15 km, whereas the earthquakes located in a belt parallel to the coastline, about 30–60 km inland (dashed outlines in Fig. 1), are generally deeper, with hypocentres in the middle crust at depths often exceeding 20 km.

The earthquakes' focal mechanisms from the Croatian focal mechanism database (Herak and Herak, 2023, personal communication; Fig. 1b) show dominance of reverse faulting mechanisms, which is expected in the compressional tectonic regime. Favourably oriented strike-slip faults are also occasionally activated. Normal faulting is exceedingly rare – in fact, the first three earthquakes in this area with reliably determined normal faulting mechanism are the three aftershocks from the Berkovići 2022 earthquake series presented in this paper.

2.2. Tectonic and geological setting

Epicentral area of the Berkovići 2022 earthquake sequence is in the south-eastern part of the External Dinarides fold-thrust belt formed along the north-eastern margin of the Adriatic microplate by prevailingly SW-directed thrusting that culminated during Middle Eocene–Oligocene times (Fig. 2a; Schmid et al., 2020; Balling et al., 2021a and references within). Structurally, the epicentral area is in the High Karst unit, which is to the NE overthrusted by the Pre-Karst unit of the Internal Dinarides, while to the SW it thrusts over the Dalmatian unit, i.e., the most external tectonic unit of the External Dinarides thrusted over the

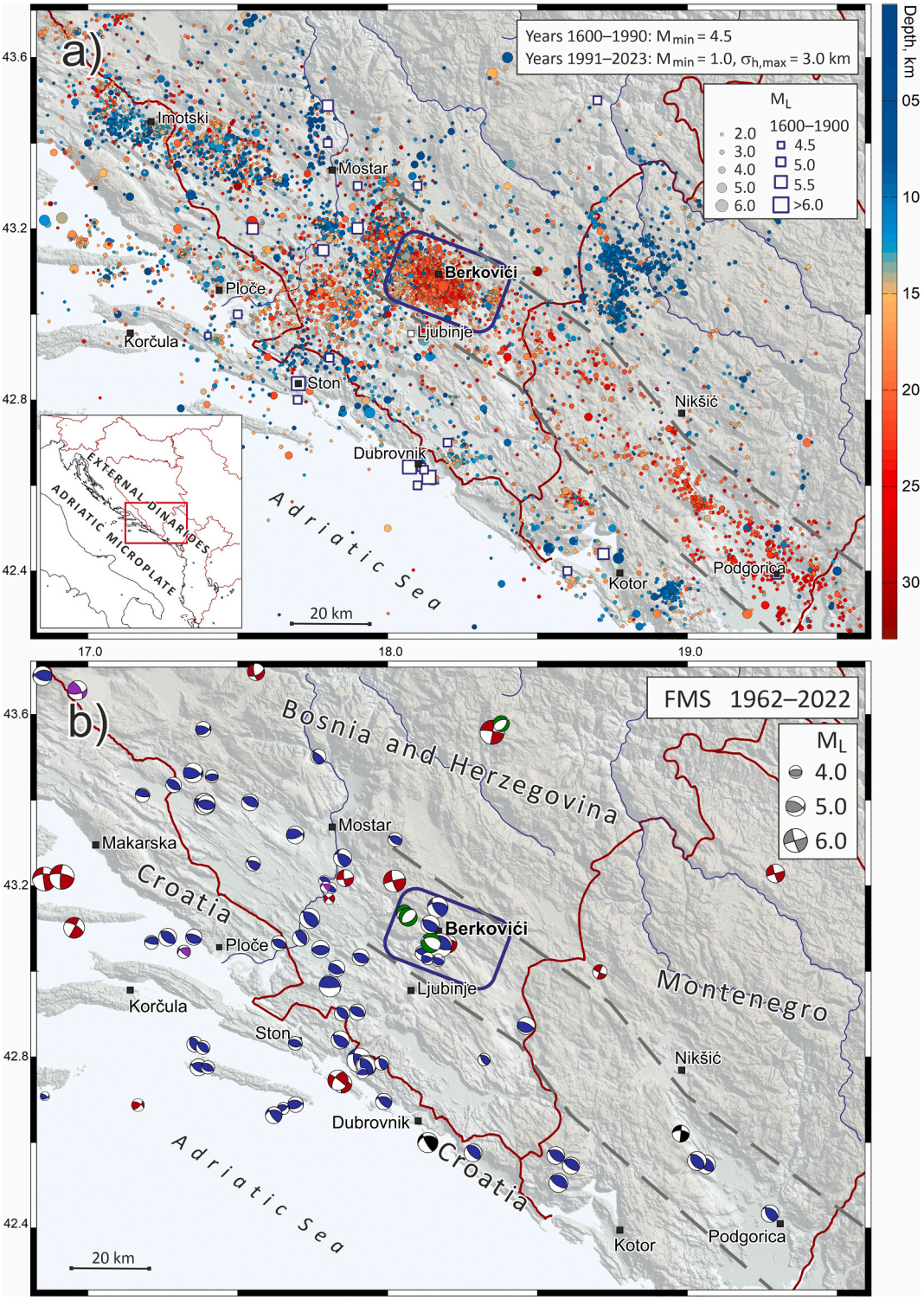

Fig. 1. (a) Seismicity in the greater area of the Berkovići 2022 earthquake series (blue outline). Epicentres of all earthquakes in the Croatian Earthquake Catalogue are shown satisfying criteria given in the top right corner (M_{min} – minimum local magnitude; $\sigma_{h,max}$ – maximum allowed standard error for the epicentre). Historical events (1600–1900) are shown as white squares (see the legend). Focal depth is indicated by the colourscale, and the symbol size scales with magnitude. Thick grey dashed lines delineate a zone of mid-crustal events. The red rectangle in the inset map shows the geographical position of the region presented in this figure. (b) Focal mechanism solutions (FMS) are from the Croatian FMS-database (Herak and Herak, 2023, personal communication; Herak et al., 2016) for the years 1962–2022. The style of faulting is colour-coded by the colour of the compressional quadrant (blue – reverse, red – strike-slip, green – normal, violet – transpression, black – unknown). The sizes of beachballs scale with magnitude. (For interpretation of the references to colour in this figure legend, the reader is referred to the web version of this article.)

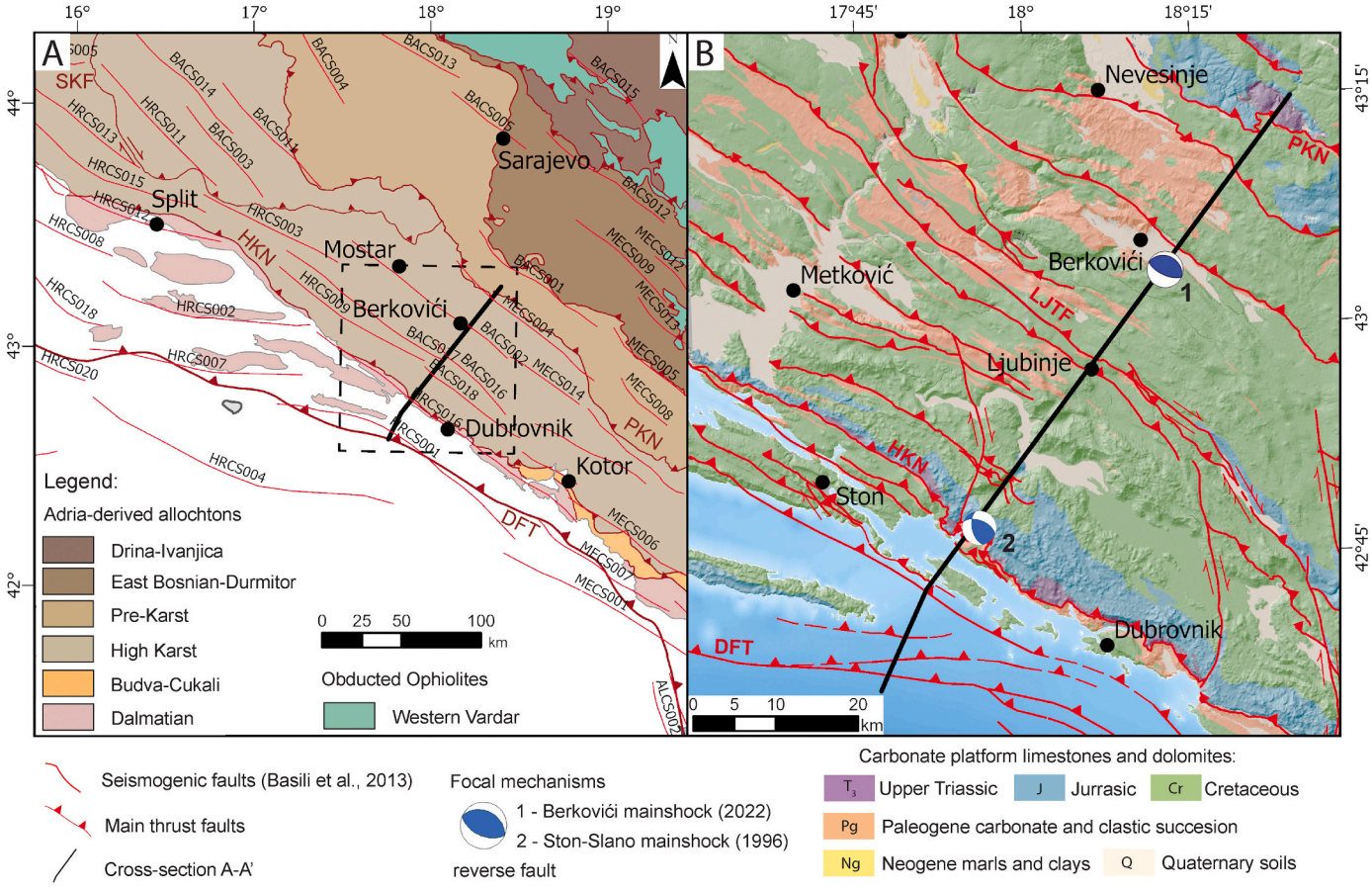

Fig. 2. (a) Tectonic map of the wider study area (after Schmid et al., 2020) and traces of seismogenic sources from The European Database of Seismogenic Faults (SHARE; Basili et al., 2013). (b) Simplified geological map compiled from the Basic Geological Map of SFRY, sheets: Trebinje (Natević and Petrović, 1967), Nevesinje (Mojičević and Laušević, 1969), Dubrovnik (Marković, 1971), Metković (Raić et al., 1975) and Ston (Raić et al., 1980), supplemented by own field measurements and by interpretation and correlation with 2D reflection seismic cross-sections (DFT – Dalmatian unit frontal thrust, HKN – High Karst nappe frontal thrust, LJTN – Ljubinje–Trebinje nappe, PKN – Pre-Karst nappe frontal thrust). Focal mechanism **1** is from this study, the solution **2** is from the Croatian focal mechanisms database (Herak and Herak, 2023, personal communication).

Adriatic foreland (Fig. 2a). On the surface, the High Karst and the Dalmatian units are mostly composed of Mesozoic shallow-marine limestones and dolomites derived from the Adriatic carbonate platform (Vlahović et al., 2005), overlain by Paleocene–Middle Eocene limestones and/or by Middle Eocene–Oligocene flysch-type and alluvial fan deposits (Fig. 2b; Natević and Petrović, 1967; Mojičević and Laušević, 1969; Raić et al., 1975, 1980; Marković, 1971). These deposits, regionally widespread and known as the External Dinarides Flysch and the Promina Beds, respectively (e.g., Babić and Zupanič, 2008; Vlahović et al., 2012; Balling et al., 2021a), are considered as *syn*-tectonic, foreland basin deposits, thus constraining the main tectonic phase in this part of the External Dinarides to Middle Eocene–Oligocene times. In the wider epicentral area, the High Karst and Dalmatian units are internally imbricated by local- to regional-scale NW–SE striking and SW-verging thrusts and reverse faults, associated by anticlines and synclines cored by Mesozoic carbonates and Eo-Oligocene deposits, respectively (Prtoljan et al., 2007; Balling et al., 2021a).

Following the main Eo-Oligocene tectonic phase in the External Dinarides, the whole Dinarides mountain range experienced a post-tectonic Oligocene–Miocene (28–17 Ma) regional uplift, assumed to have been driven by the post-collisional mantle delamination of the Adriatic lithosphere (Belinić et al., 2020; Balling et al., 2021b). Since that time, there is no substantial orogen-scale shortening observed in the External Dinarides, except for locally documented deformation accommodated by NE-dipping thrust and reverse faults associated by NW-striking dextral faults that either reactivate or cut across older Eo-Oligocene tectonic contacts (van Unen et al., 2019a, 2019b).

Historical and instrumentally recorded seismicity in this part of the External Dinarides is attributed to numerous seismogenic sources delineated and parametrized in the latest version of the European SHARE database (*URL2*, 2023), partly also presented in Kastelic et al. (2013, and references within) and in papers of Kuk et al. (2000), Kastelic and Carafa (2012), Govorčin et al. (2020) and in Schmitz et al. (2020). Seismogenic sources in the wider epicentral area of the Berkovići 2022 earthquake sequence listed in the SHARE database are shown in Fig. 2a. They are characterized by relatively small slip-rates between 0.15 and 2.01 mm/yr and inferred maximum expected magnitude (M_{max}) between 5.5 and 7.5 (Kastelic and Carafa, 2012; Kastelic et al., 2013). Besides instrumentally recorded seismicity in this area, palaeoseismic activity is also locally documented here by co-seismic uplift events in the Dubrovnik archipelago (Faivre et al., 2021a, 2021b; Faivre et al., 2023), all driven by convergence of the Adriatic plate towards the Europe, presently at GPS-derived shortening rates of ≈3–5 mm/yr (Grenerczy et al., 2005; Bennett et al., 2008; Weber et al., 2010).

3. Data and methods

3.1. Instrumental data

Earthquake locations were calculated using phase-onset times read from the seismograms gathered from several seismic networks, both permanent and temporary. The majority of seismograms come from the

permanent Croatian seismic network (network code CR; see list of DOIs in References after network codes). In the earliest sequence, and for the largest events, we also used recordings from stations in the neighbouring countries (network codes HU, IV, MN, NI, OE, SJ, SL, WS, Z3) as available on EIDA (2022–2023; see list of DOIs in References after network codes). However, by far the most relevant for this earthquake series were data collected by the semi-permanent Du-Net seismic network (*URL3, 2023*) established in November 2021 and operated by the Andrija Mohorovičić Geophysical Institute of the Department of Geophysics, Faculty of Science, University of Zagreb (Fig. 3) within the DuFAULT project. The DF03 station was installed in Nevesinje in Bosnia and Herzegovina on 4 May 2022 to improve the location precision and accuracy of the Berkovići 2022 earthquake sequence, especially to narrow the azimuthal gap towards the north. At the end of the analysed period, the network consisted of six stations equipped with high-sensitivity broadband seismographs.

To improve monitoring of this sequence, Croatian Seismological Survey from the Department of Geophysics, Faculty of Science, University of Zagreb installed three seismic stations between 24 and 27 April 2022 in the southernmost part of Croatia, close to the border with Bosnia and Herzegovina. Two of them, PM31 and PM32, were equipped with a broadband sensor and a collocated strong motion instrument, whereas only an accelerograph was installed at PM33.

Unrelated to the sequence, ETH Zürich deployed 20 BB seismic stations in Bosnia and Herzegovina within the AdriaArray initiative (network code Y5; *URL4, 2023*): ten of them 13–17 June 2022 and the other ten 18–22 July 2022. However, we began using these data in our analysis in October 2022 when they became available. In mid-October 2022, the University of Bergen and NORSAR with the Department of Geophysics, Faculty of Science, University of Zagreb installed 12 broadband stations in the southern part of Croatia within the project CRONOS (Norway Grant 2021–2024; *URL5, 2023*) and the AdriaArray initiative (network code 9H; *URL4, 2023*). These data were used in the analyses soon after the deployment.

3.2. Data analysis

All available seismograms for the period 22 April 2022–22 January 2023 were analysed using the SANDI interactive seismogram analysis program (Orlić et al., 2007–2021) for phase-picking and data organisation. Experienced seismologists picked the phase onset times manually. Local magnitudes (M_L) were estimated as described in detail by Herak (2020). The moment magnitudes (M_W) were retrieved from the **European-Mediterranean Seismological Centre** (EMSC; URL6, 2023). To reduce the influence of local conditions below each station and the influence of spatial variation of travel times relative to the theoretical ones for the chosen 1D model (e.g. Richards-Dinger and Shearer, 2000; Nooshiri, 2019), the source-specific station corrections (abbreviation SSSC) were used in the process of locating the earthquake hypocentres. In general, if the velocity model predicts reasonably accurate travel times, the locations obtained using SSSCs will be better, more robust, and less dependent on the particularities of the chosen model.

3.2.1. Earthquake location method

Earthquake foci were determined in the two-stage iterative procedure applying SSSCs obtained with the latest version of the guided grid-search *Hyposearch* programme (the first version described by Herak, 1989). In the first stage, all locations are computed assuming the best

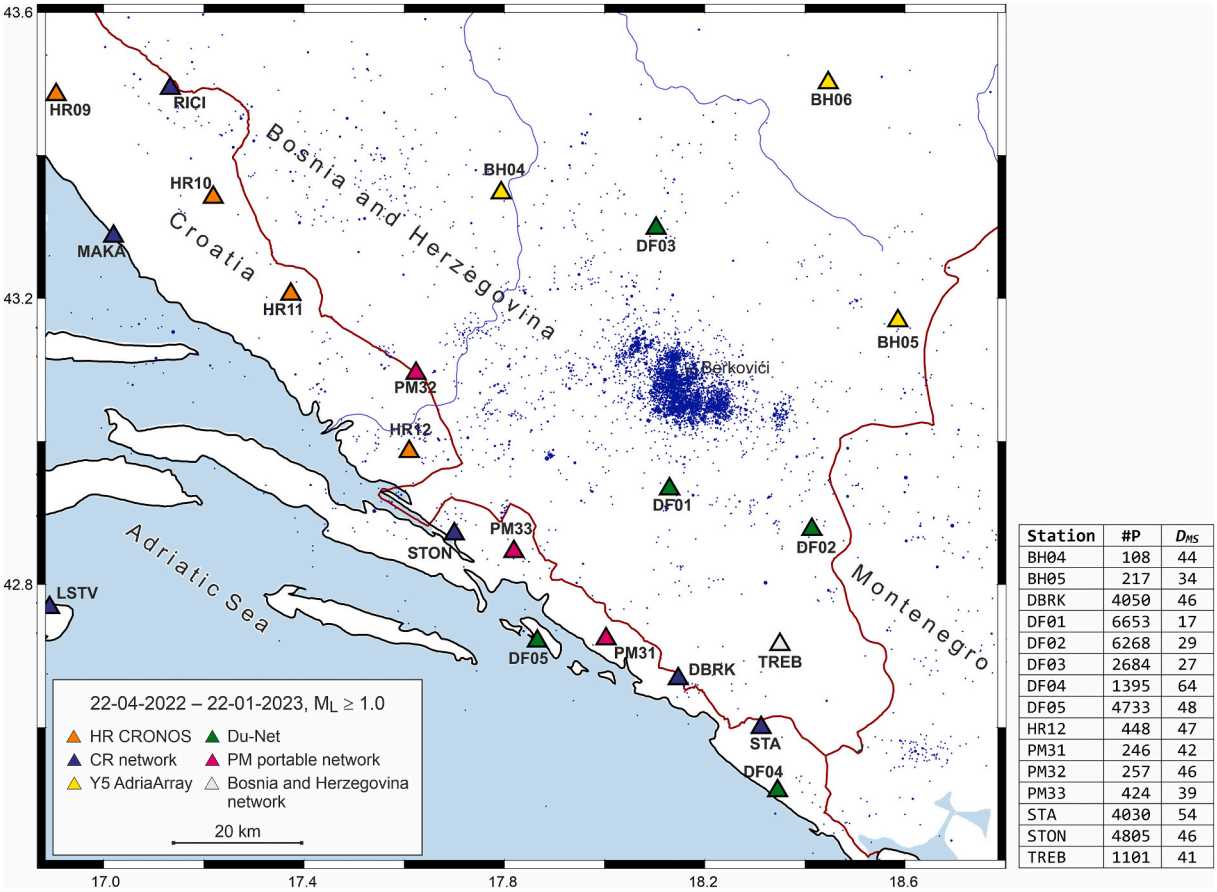

Station	#P	D_{MS}
BH04	108	44
BH05	217	34
DBRK	4050	46
DF01	6653	17
DF02	6268	29
DF03	2684	27
DF04	1395	64
DF05	4733	48
HR12	448	47
PM31	246	42
PM32	257	46
PM33	424	39
STA	4030	54
STON	4805	46
TREB	1101	41

Fig. 3. Map of the closest seismic stations (triangles) used in the earthquake analysis – each colour represents different seismic network according to the legend. Blue dots represent earthquake epicentres. The table to the right gives the number of the first P-phase readings (#P), and the distance to the mainshock (D_{MS}, in km) for the 15 closest stations. (For interpretation of the references to colour in this figure legend, the reader is referred to the web version of this article.)

known 1D velocity model used for location of events in the area. In the second stage, SSSCs are computed as the average of observed travel-time residuals for each [event–station–phase–source volume] quadruplet, which are then subtracted from the corresponding observed travel times. The source volume is determined for each event, station, and phase by the maximum correlation distance (R_{max}) from the corresponding hypocentre as obtained in stage 1. This procedure is repeated until the chosen misfit function stabilises. For a detailed description of the method, see Herak et al. (2021) and Herak and Herak (2023).

This procedure can be run several times always choosing a different velocity model and/or a different set of programme control parameters (PCP, e.g. definitions of various weighting schemes, the choice of R_{max} and misfit function, etc.). Each run will produce distinct sets of locations, frequently exhibiting closely comparable overall measures of goodness-of-fit, such as the standardized median absolute deviation (SMAD) or the mean absolute value of residuals for all picks across all earthquakes. In such instances, one can designate the most probable or representative location for each event as the weighted mean derived from all locations for that event across various runs. The weights are contingent upon the values of the selected measure of goodness-of-fit, such as SMAD, in each respective run. Such an approach also allows for estimation of epistemic uncertainty (due to imperfect knowledge of input parameters in the inversion) of each solution. We estimated the epistemic uncertainty for the epicentre (ε_E) of each earthquake as the 90th percentile of the distribution of distances from the representative (average) location. In the same way, we calculate the epistemic uncertainty for the depth (ε_h). The aleatory variability of locations, primarily arising from imperfect picks and the anisotropy of travel times not resolved by SSSC, serves as an additional indicator of confidence for each location. For some earthquake, this variability is calculated as the average of the parameters of the 1σ confidence ellipses estimated in each location run (see also Herak and Herak, 2023).

In this study, the initial 1D velocity model is based on the one used at the Department of Geophysics in routine earthquake locations in these parts of Croatia and Bosnia and Herzegovina. It was coarsely tuned in several test runs to minimise observed average absolute residuals for the phases considered (Pg, Sg, Pn, Sn; Table 1). The procedure of locations as described above required a run of seven cycles of locations and SSSC computations to stabilise the results. To assess the epistemic uncertainty of locations, we have performed additional 53 runs, each with a distinct set of models and/or PCPs. The models were derived from the initial model of Table 1, by increasing or decreasing velocities in the upper crust and/or the uppermost mantle by 1%, thus defining nine alternative models. Of the PCPs, we varied the maximum correlation distance (R_{max} = 3.0, 4.0, 5.0 or 7.0 km), and the choice whether to use the first-order correction for the average Moho dip towards each station or not. Other parameters were kept at values that produced reasonable results in several previous studies (e.g. Govorčin et al., 2020; Herak et al., 2021; Herak and Herak, 2023).

Table 1
Initial model used in the location procedure. *Vp* – P-wave velocity; Vs – S-wave velocity. Velocities were increased/decreased by $\Delta Vp,s = \pm$ 1% in all of the upper crust (layers 1–5) and the uppermost mantle (layers 8–10) to define nine alternative models.

Layer No.	Depth (km)	*Vp* (km/s)	*ΔVp* (km/s)	*Vs* (km/s)	*ΔVs* (km/s)
1	0.0	3.30		1.85	
2	1.3	4.90		2.85	
3	3.0	5.75	(± 1%)	3.25	(± 1%)
4	19.0	5.80		3.45	
5	30.0	5.90		3.50	
6	30.0	6.30	/	3.68	/
7	45.0	6.85	/	4.00	/
8	45.0	8.00		4.45	
9	65.0	8.05	(± 1%)	4.60	(± 1%)
10	95.0	8.10		4.66	

3.2.2. Aftershock magnitude and occurrence time distributions

Aftershock magnitude distribution is calculated fitting the Gutenberg-Richter (GR) relation

$$logN = a - bM_L. \tag{1}$$

Here N is the number of earthquakes with magnitude larger or equal to M_L (with $M_L \geq M_c$, M_c being the magnitude completeness threshold of the catalogue), and a and b are coefficients. The coefficients were derived in standard way using the maximum likelihood method.

The aftershock rate is modelled assuming validity of the modified Omori law (Utsu, 1961):

$$n(t) = \frac{K}{(t+c)^p}, \tag{2}$$

where $n(t)$ is the number of aftershocks that occurred in the unit of time (aftershock rate), t is the time elapsed since the mainshock. The coefficient K is productivity that depends on the magnitude of the mainshock, c is a constant that shifts the timescale to skip aftershocks that occurred too early in the mainshock's coda to be counted, and p is exponent usually between 0.7 and 1.5. We calculated the aftershock rate for the window width of 25 earthquakes with the shift of 10 earthquakes.

3.2.3. Focal mechanism solutions (FMS)

Double-couple focal mechanisms that best describe sets of manually picked polarities and/or amplitudes of the first P-phase motion on the vertical seismogram component were determined by the first-motion polarity method (FMP). All available data from local and regional networks were used.

The best fitting double-couple parameters were sought by exhaustive grid-search for the triplet (φ_o– strike, δ_o – dip, λ_o – rake) that minimizes the misfit function D defined for N observations as

$$D(\varphi,\delta,\lambda) = \frac{\sum_{i=1}^{N} w_i [r_i(\varphi,\delta,\lambda) - p_i]^2}{\sum_{i=1}^{N} w_i} \frac{1}{g(\varphi,\delta,\lambda)}. \tag{3}$$

For each station (i), r_i is the theoretical radiation pattern amplitude, p_i is the observed normalized amplitude of the P-wave first onset, and w_i is the corresponding weight. The observable p is usually simply ± 1 (polarity), but it may also be discretized into any number of classes between 0.0 and $\pm$ 1.0 indicating the amplitude of the first swing. For instance, 0.1, 0.5, 0.9, may signify the first amplitudes that are qualitatively described as “very small” (probably close to the nodal plane), “average”, and “very large” (probably close to the center of the quadrant). r is discretized in the same way as p. The individual weights w_i depend on the quality of the first onset, and the proximity of the station to the currently tested nodal plane. g is the percentage of correct polarities for the choice (φ, δ, λ) (ranging from 0.5 to 1.0) which, among similar solutions, gives preference to the ones with larger number of correct polarities.

For comparison, we also present the moment tensor best double-couple (MT) solutions for three earthquakes from this sequence as reported by various international agencies: the *Istituto Nazionale di Geofisica e Vulaconologia* (*INGV*, 2022), the *Deutsches GeoForschungsZentrum* (*GFZ*, 2022), the *Observatoire de la Côte d'Azur* (*OCA*, 2022), the Global Centroid-Moment-Tensor (CMT) Project (*GCMT*, 2022), and the U.S. Geological Survey (*USGS*, 2022).

3.3. Geological data and regional cross-section modelling

To gain a better understanding of the Berkovići earthquake sequence and to delineate potential seismogenic source we constructed a regional geological cross-section, which includes Dalmatian, High Karst, and part of Pre-Karts tectonic units, Berkovići and Ston–Slano epicentral area (thick solid lines in Figs. 2). For this purpose, we digitized in ArcGIS Pro

3.1 Basic Geological Map of SFRY, sheets: Trebinje (Natević and Petrović, 1967), Nevesinje (Mojičević and Laušević, 1969), Dubrovnik (Marković, 1971), Metković (Raić et al., 1975) and Ston (Raić et al., 1980). Important deformation structures and faults with significant displacement were singled out by analysing the maps, which were further inspected during the field observations to cross-check available structural measurements and structural relations of stratigraphic units, to fill up the gaps with no structural data and to determine kinematic indicators if available. For the offshore area, faults were mapped based on 2D seismic cross-sections provided by Croatian Hydrocarbon Agency. Simplified geological map of wider research area is shown in Fig. 2b, where map units are grouped based on their age and only most important faults are presented.

Construction of regional geological cross-section was done within the Petex MOVE 2019.1 structural modelling software. Input data were: 1) European digital elevation model (EU-DEM 1.1, 2022) and Bathymetry Digital Terrain Model (EMODnet Bathymetry Consortium, 2022); 2) offshore 2D seismic cross-section, provided by the Croatian Hydrocarbon Agency; 3) digitized map representing stratigraphic units, faults and deformation structures imported from GIS project; 4) structural measurement data from the maps and those gathered in the field, which were additionally digitized within the Petex MOVE 2019; and 5) lithostratigraphic table containing average thicknesses of each unit compiled from previously mentioned geological maps. All structural data within 2.5 km distance from the cross-section, as well as intersections with stratigraphic units and faults were projected onto topographic line that was extracted from DEM and bathymetry data. Structures were constructed starting from the youngest map units and in respect to projected structural data to accurately reflect geometry of each unit. Offshore part of the cross-section (part of the Mljet structure, for details see section 4.2 and Fig. 11) was constructed based on the interpretation of 2D seismic cross-section and correlated with surface data. For those stratigraphic units that do not outcrop at surface, average thickness was used to project them parallel to overlying unit. The geometry of the thrusts, their ramps and flats, was constructed in respect to geometry of the structures in the hanging wall. Geometry of the basal thrust of the Dalmatian unit was modelled based on the hypocentres' distribution of the 2022 Berkovići earthquake sequence, fault plane solutions of the Berkovići 2022 and Ston–Slano 1996 mainshocks, and in respect to the geometry of the basal thrust of the High karst unit and Ljubinje thrust (for details see section 4.2 and Fig. 11). Certain parts of the cross-section were retro-deformed using the fault-bend-folding and fault parallel flow algorithm within the Petex MOVE 2019 to validate the geometry of the modelled structures.

Balancing of the entire cross-section is outside the scope of this study, because to do so frontal thrust of the Dalmatian unit (ca. 30 km further to the SW) should be included in the cross-section, as well as the intraplatform basin (located SW from the Mljet structure) containing pelagic Oligocene to Miocene sediments and underlying Mesozoic carbonates for which there is no available borehole data.

4. Results and discussion

We present here the results of statistical, spatial and temporal analyses of the earthquake sequence that started on 22 April 2022 with an earthquake of local magnitude 6.0 and epicentre in the southern part of the seismically active External Dinarides. Moreover, we discuss assessed aleatory variability and epistemic uncertainty for the earthquake location parameters. We complement these analyses with the report of macroseismic intensity field of the mainshock to show its impact on the surface (Appendix A). To understand seismotectonic context, we present a constructed regional geological cross-section.

4.1. Instrumental data analyses

In the first nine months of the studied sequence, from 22 April 2022 until 22 January 2023, we located hypocentres and computed local magnitudes for 7217 earthquakes. These locations are based on a set of manually picked 102,743 phase onset times (43,746 Pg, 55,430 Sg, 1462 Pn, 2105 Sn). As a rule, whenever possible both P- and S-phases are picked. However, at more distant stations Pg (or Pn) is sometimes drowned in noise, but Sg (or Sn) is clearly visible and picked. Therefore, the number of S-phases is larger than the number of the corresponding P-phases.

The Berkovići earthquake sequence began with the $M_L = 6.0$ ($M_W = 5.7$) on 22 April 2022 21:07:48.6 UTC with epicentre location at ($\varphi = 43.066°$N, $\lambda = 18.185°$E) and at hypocentral depth of $h = 22$ km, in the Municipality of Berkovići, Bosnia and Herzegovina. The strongest aftershock occurred on 24 April 2022 04:27 UTC with $M_L = 4.9$ ($M_W = 4.7$). Table 2 shows earthquake location parameters, together with local magnitude and calculated focal mechanism solutions (for details see section 4.1.3) for eight strongest events of the sequence.

4.1.1. Epistemic uncertainty and aleatory variability of locations

To assess epistemic uncertainty of locations, we have performed 54 runs – for nine alternative models (Table 1) and four different maximum correlation distances (R_{max} = 3.0, 4.0, 5.0 or 7.0 km) – which has a significant influence on the results, and the choice whether to use the first-order correction for the average Moho dip towards each station or not. As discussed in Herak and Herak (2023), the sets of models and PCPs used here are very far from exhausting all possible reasonable combinations of parameters. In fact, considering the number of parameters that define each run, it would be an impossible task. This renders our epistemic uncertainties not conservative and probably underestimated. However, it is a step forward towards better quantification of epistemic uncertainty of locations, which is often neglected in similar studies.

The 54 resulting different sets of locations are all characterized by similar overall goodness-of-fit measures. For example, the standardized median absolute deviation (SMAD) of residuals for all phases is found to vary between 0.12 s and 0.13 s. This difference of up to 0.01 s is equal to the best possible accuracy of phase picking, so we consider all sets of locations equally valid and assign unit weights to all of them. Thus, the simple means of the hypocentral coordinates and origin times of the 54 runs were taken as their representative values. Likewise, the epistemic uncertainties (ε_h and ε_z for the epicentre location and focal depth, respectively) for each event were determined as the unweighted 90-percentile of the distribution of distances of 54 foci from the representative (average) one and were included as such in the final earthquake catalogue. Aleatory variation a_h of the epicentral coordinates is estimated for each event as the mean of the lengths of the major semi-axis of the 90%-confidence error-ellipse of the 54 individual solutions.

In Fig. 4, we show the temporal variation of the location uncertainty measures (horizontal aleatory uncertainty, epistemic uncertainties of the epicentre and of focal depth) estimated as the mean value of the corresponding quantity in a sliding window containing 25 consecutive events for $M_L \geq 0.5$. There is a clear decrease of the mean horizontal aleatory uncertainty on 4 May 2022 when the DF03 station in Nevesinje, 26 km to the north-northwest from the mainshock, was deployed to monitor this sequence, thus primarily narrowing the azimuthal gap. Periods of increased uncertainty correlate well with the times when the closest stations (DF01, DF02, DF03) had problems that could not be resolved immediately, resulting in loss of data. This is especially true for the closest station DF01 (15 km from the epicentre), and the effect is most clearly observed for the uncertainty of the focal depth (ε_z, Fig. 4c), which increases from <1 km to >5 km.

4.1.2. Statistical, temporal and spatial analyses

The analysis of the frequency-magnitude distributions (Fig. 5), i.e. the Gutenberg-Richter relation, shows that the catalogue can be considered complete for magnitudes $M_L \geq M_C = 1.3$. The Gutenberg-Richter coefficient b equals 1.07, still within the usual range of values,

Table 2
Focal mechanism parameters for the eight considered earthquakes computed using the first-motion polarity method. t_0 is origin time of the event, φ and λ are geographical coordinates of the epicentre, h is the focal depth, and M_L is event's local magnitude. φ_i, δ_i, λ_i, are the strike, dip and rake of the two nodal planes, respectively (indices 1, 2; no preference of solution implied) or the P and T-axes (indices P, T). Q stands for quality of solution (1–5, 5 being the best).

	t_0 (UTC)	φ [°N]	λ [°E]	h [km]	M_L	φ_1 [°]	δ_1 [°]	λ_1 [°]	φ_2 [°]	δ_2 [°]	λ_2 [°]	φ_P [°]	δ_P [°]	φ_T [°]	δ_T [°]	Q
1	22.4.2022 21:07:48.6	43.066	18.185	21.6	6.0	109	67	87	297	23	97	201	22	13	68	5
2	23.4.2022 00:59:08.0	43.134	18.057	15.9	3.9	45	43	−109	250	50	−72	223	77	328	4	2
3	23.4.2022 02:20:27.2	43.136	18.065	13.8	4.5	215	45	−109	61	48	−71	42	77	138	2	4
4	23.4.2022 02:34:21.0	43.036	18.121	21.7	3.7	271	27	71	112	65	99	195	19	41	69	4
5	24.4.2022 04:27:53.4	43.066	18.144	24.5	4.9	271	43	−125	135	56	−61	99	66	205	7	3
6	5.5.2022 22:27:06.9	43.027	18.144	20.7	3.0	57	45	43	294	61	126	359	9	254	57	5
7	2.12.2022 20:05:05.3	43.118	18.141	21.8	4.5	295	59	79	136	33	108	33	13	176	74	3
8	10.12.2022 23:12:54.3	43.031	18.168	21.6	3.2	287	59	87	113	31	95	19	14	188	76	3

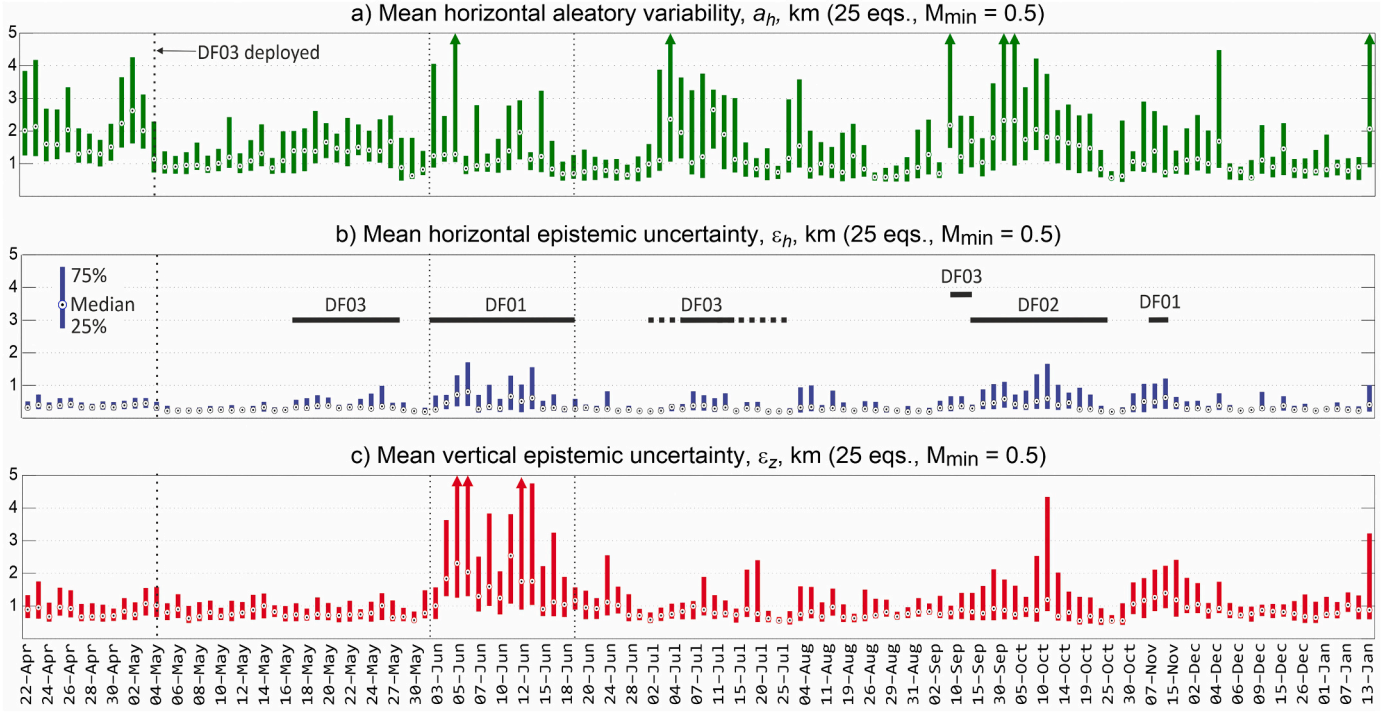

Fig. 4. Temporal variation of the location uncertainty measures estimated as a mean value of the corresponding quantity in a sliding window containing 25 consecutive events with $M_L \geq 0.5$. (a) Mean horizontal aleatory variability (major half-axis of the 90% confidence ellipse). (b) Mean epistemic uncertainty (90-percentile radius) of the horizontal coordinate. (c) Mean epistemic uncertainty of the focal depth (90-percentile radius). Bars topped with arrows indicate values larger than 5 km. Periods of increased uncertainty correlate well with the times when the closest stations were out of order marked with horizontal bars and indication of the missing seismic station. Dashed lines within the bar indicate periods of intermittent recording due to unstable power supply. Note that the time scale is not equidistant!

which suggests 11.8-fold increase of number of events per one unit of magnitude decrease.

The temporal analysis of the sequence modelled for earthquakes $M_L \geq 1.3$ with the modified Omori law (Fig. 6) shows the decrease in earthquake rate from about 2000 events/day in a few hours after the mainshock to about one event per day at the end of the analysed period. The decay rate exponent $p = 1.2$ is within the normally expected range of values. With this rate, after one year since the beginning of the series, we can expect five earthquakes with $M_L > 1.3$ in 10 days, and one such event per month on the average can be expected after about 10 years. The decrease in earthquake rate is monotonous and the fitted line follows the data nicely until 224 days after the mainshock – when aftershock $M_L = 4.5$ of 2 December 2022 occurred and activity increased in the following weeks (Fig. 6). The epicentre of this aftershock was 7 km away from the mainshock's, in the area that has been active since the beginning of the sequence (see earthquake subgroup *c* in Figs. 7 and 8 and event No. 7 in Table 2).

4.1.3. Earthquake locations

Epicentres of all located events of the Berkovići sequence are shown in Fig. 7a. The aftershocks seem to group into four distinct earthquake clusters (subgroups *a–d* in Figs. 7a and 8). Figs. 8a and 9 show only earthquakes with more reliable locations and provide more detailed insight into the structure of aftershock clustering. Subplots 7b and 7c show heat-maps of the number of earthquakes and the cumulative moment release, respectively, whereas Fig. 8 presents spatio-temporal evolution of the sequence. The distribution of the number of aftershocks reveals that hotspots do not correspond with the locations of more intense events. This suggests that the stronger earthquakes predominantly dissipated stress in proximity to their foci, with subsequent aftershock activity occurring further away on the activated faults.

The main cluster (*a* in Figs. 7a and 8) is found in the area around the mainshock where the bulk of aftershocks occurred on the causative fault. It is ≈15 km long (in the WNW–ESE direction) and ≈8 km wide (NNE–SSW). Most aftershocks with $M_L > 3.0$ occurred WSW and S of the

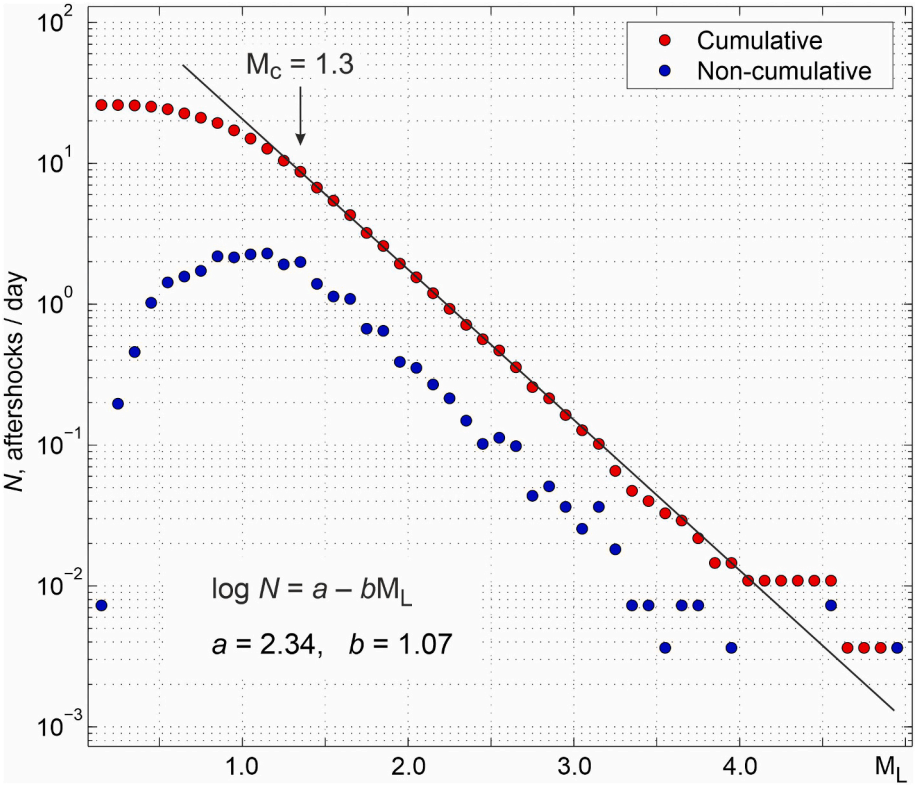

Fig. 5. Frequency-magnitude distribution for the first nine months of the Berkovići earthquake sequence (mainshock excluded). Blue circles represent non-cumulative distribution while red circles present cumulative distribution. The aftershock catalogue may be considered complete for $M_L \geq 1.3$. The black solid line is the fit of the Gutenberg-Richter relation with the coefficients $b = 1.07$ and $a = 2.34$. (For interpretation of the references to colour in this figure legend, the reader is referred to the web version of this article.)

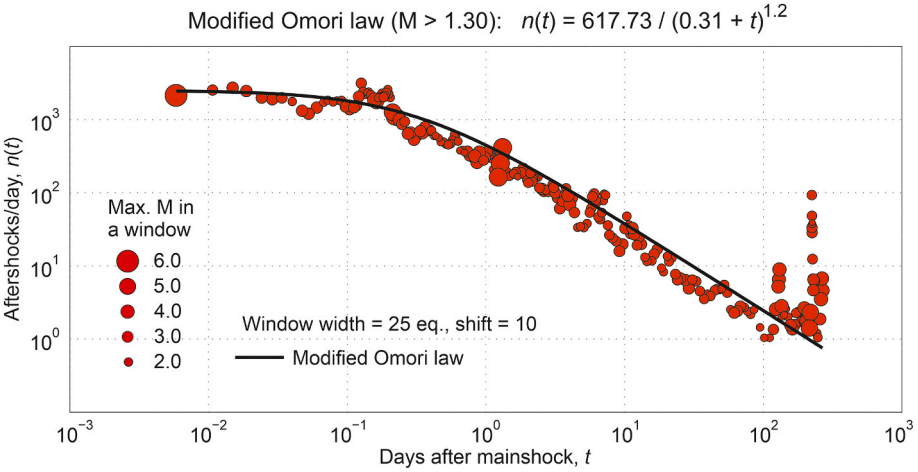

Fig. 6. Temporal activity rate variation for events with magnitude $M_L > 1.30$: fit of the modified Omori law (solid black line) in log-log scale. The size of the circle depicts the largest earthquake in a window for which the earthquake rate was calculates.

mainshock. Fig. 8 shows that this subgroup was active throughout the whole analysed time span, however, smaller temporal-spatial clusters are seen within it. For instance, cluster a_1 just north of Vlahovići in Fig. 8a and b was active in late August and early September 2022. A detailed analysis of possible subclustering is outside the scope of the study.

Subgroup *b* is further away to the northwest (≈12 km from the mainshock), just to the SE of the village Dabrica, and encompasses aftershocks that form a SW–NE oriented cluster (perpendicular to the Dinaric strike). This area was activated shortly after the mainshock occurred and has been active throughout the whole analysed period. However, almost half of the located events (≈250 earthquakes) occurred during April 2022. The strongest aftershocks in this cluster happened on 23 April 2023 at 00:59 and 02:20 with magnitudes 3.9 and 4.5 and at depths of 16 and 14 km, respectively. A small cluster within this subgroup occurred close to intersection with subgroup *c* in the period 10–13 November 2022 (with the strongest earthquake of $M_L = 3.5$), in a way "announcing" the forthcoming activity within subgroup *c*.

Subgroup *c*, to the north of the main subgroup and close to the village of Trusina (≈6 km north of the mainshock), was initially active in April

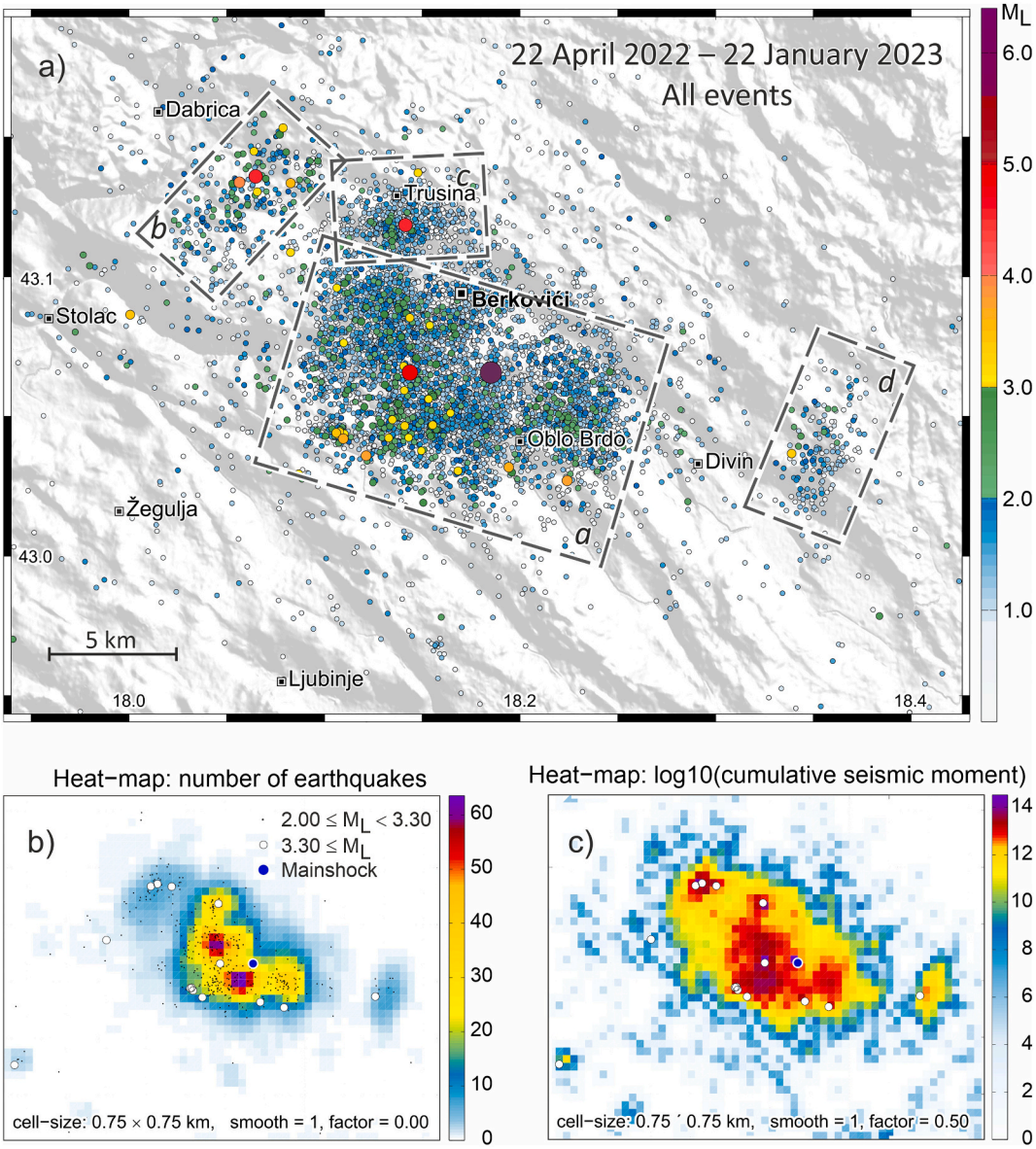

Fig. 7. (a) Epicentres of all 7217 located events in the first nine months of activity. Local magnitude is indicated by the colour scale on the right. The four distinct epicentre subgroups *a*–*d* are shown by dashed rectangles. (b) Heat-map presenting number of located events within each cell (0.75 km × 0.75 km). Moderate spatial smoothing involving only the neighbouring cells was applied. (c) Heat-map of logarithm of cumulative seismic moment released in each cell (0.75 km × 0.75 km). Weak spatial smoothing was applied (only neighbouring cells, with unsmoothed field weight factor = 0.5).

and May 2022; however, the main activity started on 2 December 2022 at 20:55 with M_L = 4.5 aftershock (see Fig. 8). Between 2 and 4 December 2022, 310 small events were located there.

The farthest subgroup (*d* in Figs. 7a and 8), with comparatively weak events is located to the east of Divin, ≈14 km southeast from the mainshock, also featuring SW–NE elongated cluster. It was active almost entirely in the first weeks of the sequence.

In general, focal depths of this sequence range between 10 and 30 km. However, majority of them (86%) had focal depths between 15 and 25 km and 61% is between 20 and 25 km of depth. These hypocentral depths are considerably larger than the typical ones for the Dinarides (5–15 km) but agree with previously observed depths of mid-crustal events in the zone stretching from this area southeastwards to Montenegro (see black dashed line in Fig. 1). Detailed description of the depth distribution is in section 4.1.4.

4.1.4. *Focal mechanisms*

The focal mechanisms have been determined as the first-motion polarity (FMP) solutions for eight earthquakes – they are presented in Table 2. The attempts to include smaller events failed because they were mostly well recorded only on a small number of the closest stations, thus rendering inversions unstable and unreliable. In Fig. 9, we show our solutions in comparison to the moment tensor best double-couple (MT) solutions for three earthquakes from the Berkovići sequence as reported by various international agencies. In general, and especially for the mainshock, FMP and MT solutions agree very well although they are related to different episodes of the faulting process.

The mainshock shows pure reverse mechanism on a fault gently dipping to the NNE (preferred solution based on the hypocentral locations, see Fig. 11). Figs. 7a and 8 reveal that the aftershock cluster *a*, roughly corresponding to the events related to the main causative fault, is unevenly populated with aftershock epicentres, with a large patch to the north and east of the mainshock's epicentre being considerably less

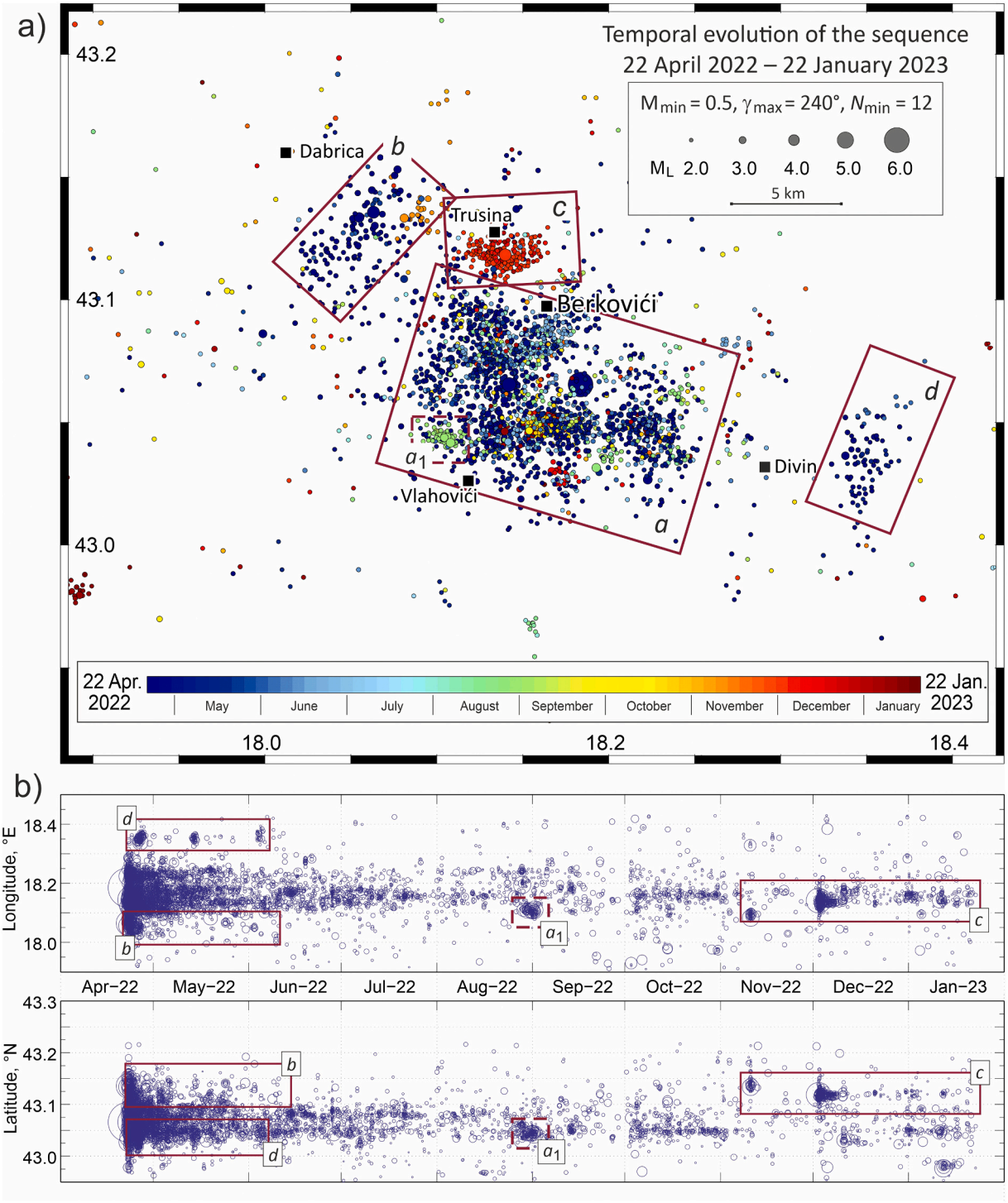

Fig. 8. Spatio-temporal evolution of the Berkovići sequence. a) Map view. The date is according to the colour-scale at the bottom, and symbols scale with magnitude. Only well-located events are shown, satisfying criteria shown in the legend (γ_{max} – maximal allowed station azimuthal gap, N_{min} – minimum number of phases used in location). b) 2D presentation. Red boxes correspond to the subgroups as shown in part a) above. The main subgroup (*a*) is not marked. A cluster (a_1) within the main subgroup *a* is shown by a dashed box as an example of possible further subdivision of the four main subgroups. (For interpretation of the references to colour in this figure legend, the reader is referred to the web version of this article.)

active than the rest of this group. It most probably corresponds to the part of the causative fault plane tentatively indicated in Fig. 9 (with dimensions estimated after Wells and Coppersmith, 1994) where most of the stress was released by the mainshock.

Similar mechanism is observed for other three earthquakes in the southern part of the main earthquake cluster *a* and for one earthquake in the cluster *c* (Figs. 7a and 8) just to the north, close to Trusina. These are somehow expected solutions, as the causative faults follow the Dinaric strike (SE–NW) prevailing in this area. However, three aftershocks seem to have been caused by normal faulting, which is unusual in the region of tectonic compression: two of them are found in the smaller subgroup of aftershocks to the south of Dabrica (*b* in Figs. 7a and 8) and one is located close to the mainshock. The first two (23 April 2022, Nos. 2 and 3 in Table 2) strike approximately perpendicularly to the Dinaric strike –

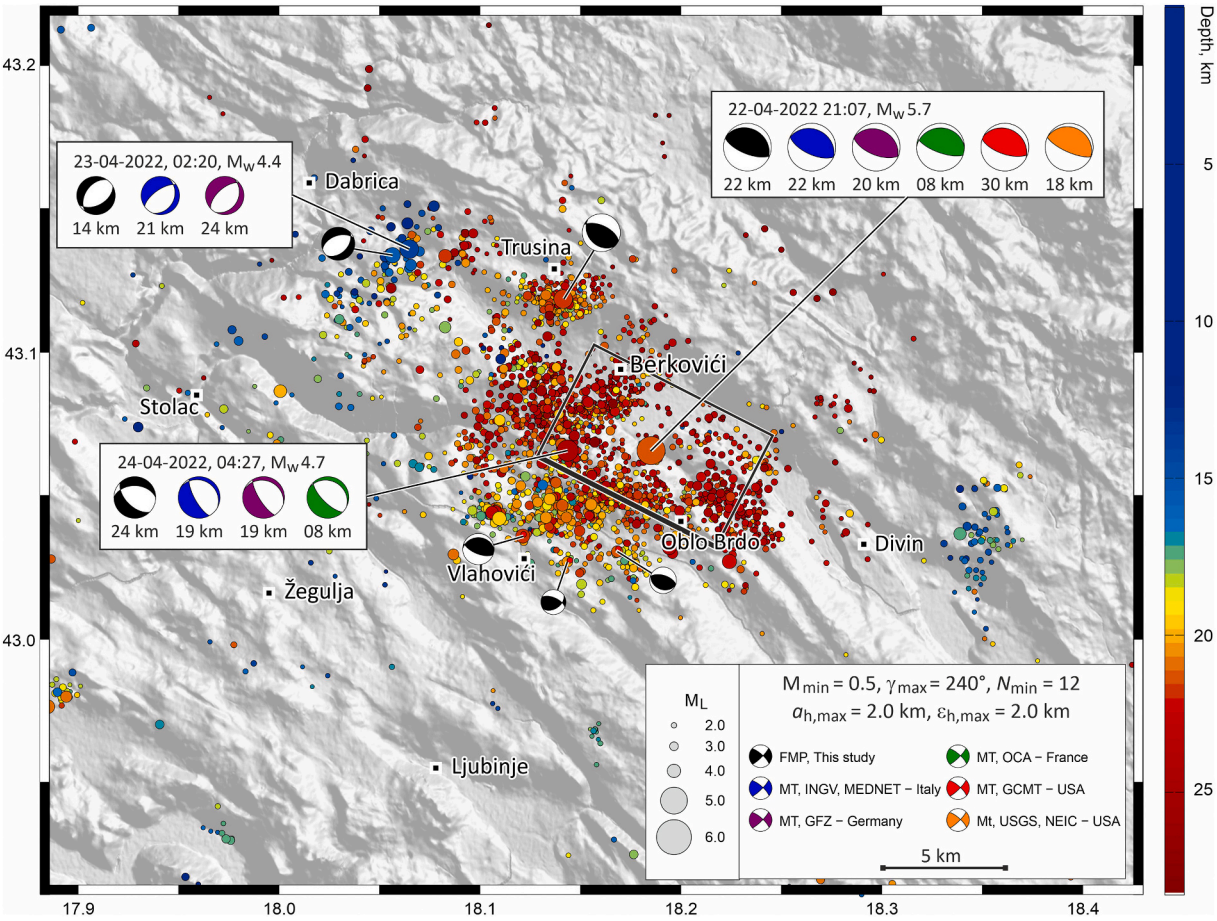

Fig. 9. Map of the earthquake epicentres in the first nine months (22 April 2022–22 January 2023) of the Berkovići sequence for only more accurately located earthquakes satisfying criteria shown in the bottom right corner. M_{min} is minimum local magnitude, γ_{max} is maximal allowed station azimuthal gap, N_{min} is minimal number of phase onset times used for location, $a_{h,max}$ is maximum allowed aleatory variability for the epicentral coordinates, and $\varepsilon_{h,max}$ is maximum allowed epistemic uncertainty for the epicentral coordinates. The symbols (circles) are scaled with magnitude, and their colour indicates focal depth according to the colour scale on the right. Solutions of the focal mechanisms for the first-motion polarity method (this study) for the eight events are shown as lower hemisphere stereographic projection. Sets of the moment tensor best double-couple solutions (MT) for three earthquakes are presented separately in white rectangles. They are colour-coded by the reporting agency, and the focal depth providing the best variance reduction during inversion is shown below each beach-ball. Black rectangle depicts the assumed plan-view (vertical projection) of the causative fault plane of the mainshock (dimensions after Wells and Coppersmith, 1994, for $M_w = 5.7$), with a thick black line denoting its shallower edge.

with the currently available data about earthquakes in this area and local geology we can speculate that redistribution of stress caused by the mainshock fracture increased the probability of (re)activation of old normal faults striking SW–NE if they exist there.

To try to verify this hypothesis, we computed the Coulomb stress change caused by the mainshock rupture using *Coulomb 3.4* program (Toda et al., 2011). As no detailed model of the slip distribution on the fault plane is available, the mainshock fault was modelled to be consistent with the focal mechanism and depth as described above, and its dimensions were estimated using the relationships from Wells and Coppersmith (1994). The amount of slip was tapered-off towards the fault edges. The modelling presented in Fig. 10 shows Coulomb failure stress (ΔCFS) increase of 0.5 bars at the location of the normal aftershock of 23 April 2022, 02:20 (No. 3 in Table 2), thus promoting rupture on the optimally oriented normal fault there with strike roughly NNE–SSW (parallel to the strikes of short black lines in Fig. 10). This approximately agrees with the observed strikes of the two nodal planes (NE–SW) of the 23 April 2022 normal events (see Fig. 9). The match is not perfect, and modelled ΔCFS is not very high, but this explanation remains the most plausible until it is confirmed or refuted by a future, more detailed Coulomb stress analyses based on the realistic slip distribution on the mainshock's fault.

The third aftershock with normal faulting (24 April 2022, No. 5 in Table 2) seems to have occurred near the edge of the same fault as the mainshock – the strike and dip of preferred solutions, especially the MT ones (see Fig. 9) agree with the mainshocks', but the rake indicates almost pure normal kinematics. Events with opposite mechanisms occurring on the same fault shortly one after another, strongly indicate a reversal of the stress state (e.g. Ide et al., 2011; Sattari, 2018). This in turn suggests total stress drop and dynamic overshoot of the rupture caused by inertial effects, thus reducing shear stress below dynamic friction (McGarr, 1999). A rather similar case of large normal aftershocks shortly following pure thrust mainshock on a gently dipping fault is suggested (albeit on a much larger scale!) for the Tohoku-Oki earthquake of 2011 by Ide et al. (2011). Opposite mechanisms in aftershock sequences have also been documented by, e.g. Beroza and Zoback (1993) for the Loma Prieta aftershocks, and Ratchkovski (2017) for the Denali fault (Alaska). A prerequisite is also that the fault zone is a compliant one, with reduced rigidity in its neighbourhood compared to the surrounding host rocks (Kang and Duan, 2015). Compliant zones develop from damage accumulation during seismic ruptures (Nie and Barbot, 2022), and fault zone lithology may play an important role in their formation (Materna and Bürgmann, 2016). If this is indeed the case, it may have implications for seismogenesis and tectonic processes

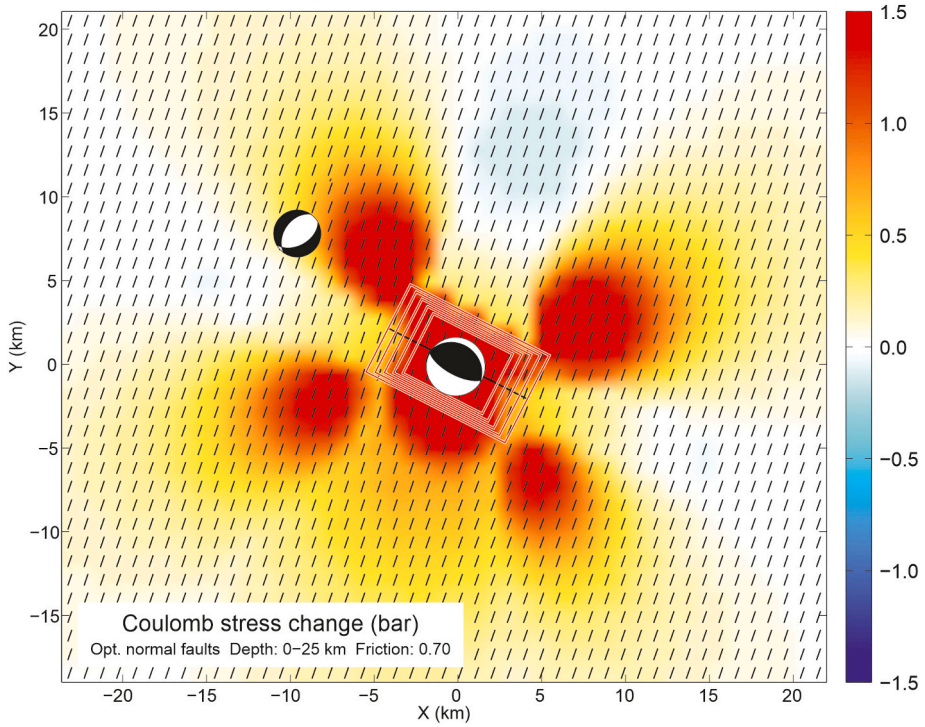

Fig. 10. The Coulomb failure stress change for optimally oriented normal faults, with the friction coefficient $F = 0.7$, caused by the mainshock rupture with a total seismic moment of 5×10^{17} Nm. The maximum stress change computed for the depths between 0 km and 25 km is shown. A generic model of the seismogenic fault is assumed, satisfying the focal mechanism and focal depth of the mainshock, with dimensions after Wells and Coppersmith (1994). The slip on the fault is linearly tapered-off towards the edges of the fault. Short lines show strike directions of the normal faults optimally oriented for failure. Overlain are the beach-ball diagrams for the mainshock and the normal event of 23 April 2022, 02:20, No. 3 in Table 2; see also Fig. 9). Computed and plotted using Coulomb 3.4 program (Toda et al., 2011).

in these parts of External Dinarides.

4.1.5. *Vertical cross sections*

To get better insight into the aftershock clustering in depth, in Fig. 11 we plot four profiles cutting through the activated hypocentral volume. In any attempt to explain the cross-sections in Fig. 11, one must be aware of rather large uncertainties (see Fig. 4) of focal coordinates (especially the depth) due to the sparseness of the local network and take care not to overinterpret the apparent geometrical trends.

Profile A in Fig. 11 shows that the hypocentres within $D_{\max} = 5$ km from the trace profile are spread in the depth range between 10 and 30 km. Most events, belonging to subgroup *a* (Figs. 7a and 8), have foci below 20 km. Rather steeply dipping cluster in the NW part of the profile corresponds to events in cluster *b* where two aftershocks with normal mechanisms are found at shallower depths. Judging from the cross-section A, the planes of the corresponding focal mechanism solutions (Nos. 2 and 3 in Table 2) dipping towards SE are more likely to be the actual fault planes. In the transverse profile B ($D_{max} = 2$ km), the western edge of the main aftershock subgroup *a* shows as a rather scattered cluster apparently dipping to the NNE with a sharp NW boundary. At its NNE-most end, it crosses the aftershock subgroup *c* which appears as a well-defined group of foci steeply dipping towards NNE, and ranging in focal depths between 17 and 25 km. The transverse profile C ($D_{max} = 2$ km) crosses through the subgroup *a* near the mainshock, and shows a cluster of foci dipping towards NNE, in agreement with one of the FMS fault-planes for the mainshock (No. 1 in Table 2). The transverse profile D ($D_{max} = 2$ km) shows the SE end of the main cluster, again suggesting a dip towards NNE.

The observed scarcity of aftershocks in the areas towards N, NE and E from the mainshock (Figs. 9 and 11), and information from cross-sections through the hypocentral volume (Fig. 11) suggest that the rupture most likely spread down-dip from the hypocentre, where most of the accumulated stress was released by the mainshock.

4.2. *Seismotectonic interpretation*

To delineate potential seismogenic source of the Berkovići 2022 earthquake sequence, hypocentres of this sequence are projected onto the constructed regional geological cross-section, including events with $M_L \geq 1$ and within 5 km distance from the cross-section (Fig. 2). In construction of this cross-section, we firstly modelled the geometry of the basal thrusts of the High Karst (labelled *BTHKU* in Fig. 12) and the Dalmatian tectonic units (labelled *BTDU* in Fig. 12), based on surface geological data and the interpretation of 2D reflection seismic section in the Adriatic offshore which was provided by Croatian Hydrocarbon Agency. Starting from the outcropping location of the frontal thrust of the High Karst unit at Slano (Figs. 2 and 12), the basal thrust of this unit is modelled by successive ramps and flats that passes downwards to the NE into a root zone decollement, modelled at the depth of 12 km and at the distance of c. 40 km from the outcropping front. A group of shallowest hypocentres of the Berkovići sequence could be attributed to this basal thrust surface, in particular those events at a vertical distance of 2–4 km above and below this thrust surface (Fig. 12).

Above this basal thrust, yet another regional-scale thrust surface is modelled within the High Karst unit (Fig. 12), indicating that this unit is here subdivided into two subunits, as documented further to the NW by Balling et al. (2021a). Starting from the outcropping front at Ljubinje, this shallower thrust surface also passes downwards to the NE into successive ramps and flats, modelled to the depth of 8 km underneath the frontal thrust of the Pre-Karst unit exposed at the surface at the NE termination of the cross-section (Fig. 12). No hypocentres of the Berkovići sequence were found close to this thrust surface.

The seismogenic source for the mainshock of the Berkovići sequence, and for the group of events closest to the mainshock, is modelled by the

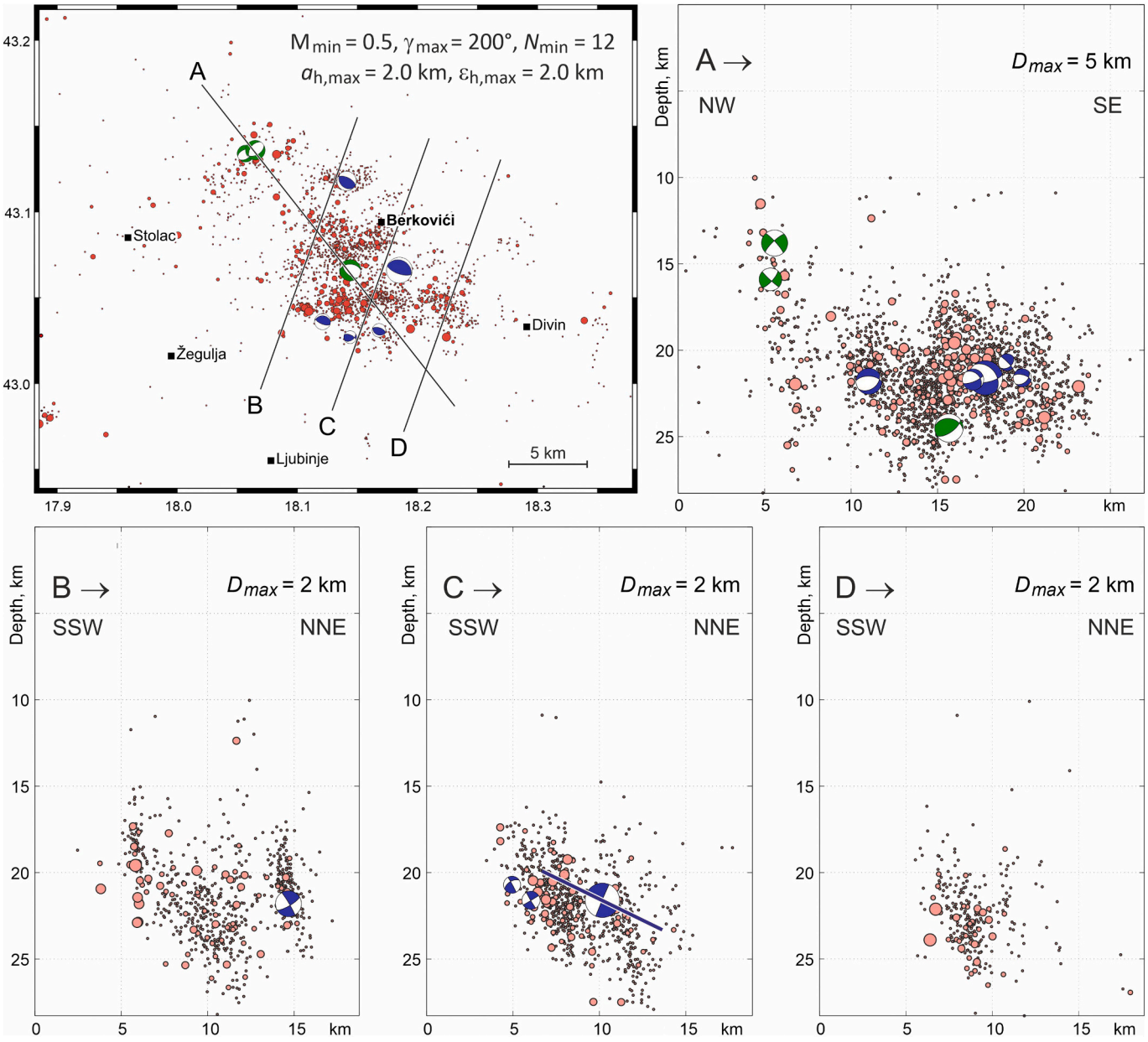

Fig. 11. Top left: Epicentres of earthquakes from the first nine months (22 April 2022–22 January 2023) of the Berkovići sequence for only more accurately located earthquakes satisfying criteria shown in the top right corner. M_{min} is minimum local magnitude, γ_{max} is maximal allowed station azimuthal gap, N_{min} is minimal number of phase onset times used for location, $a_{h,max}$ is maximum allowed aleatory variability for the epicentral coordinates, and $\varepsilon_{h,max}$ is maximum allowed epistemic uncertainty for the epicentral coordinates. Beach-balls show lower hemisphere stereographic projection of the best solution. Blue and green compressional quadrants denote reverse and normal styles of faulting, respectively, and the size scales with magnitude. A–D: Vertical cross-sections along the lines shown in the map (top left). Half corridor width (D_{max}) is given on each subplot. The FMSs in the cross-sections are shown as farther hemisphere projections in the profile plane. Blue solid line in section C is the intersection with the assumed causative fault (see Fig. 8 for its position). (For interpretation of the references to colour in this figure legend, the reader is referred to the web version of this article.)

mainshock hypocentre depth, its fault plane solution, the hypocentre distribution of closest events to the mainshock projected onto the cross-section and by the geometry of structures reconstructed in the upper part of the cross-section, i.e. above the depth of 12 km. Based on these data we firstly delineated a 23° NE-dipping ramp at the mainshock hypocentre depth of 22 km, which downwards to NE turns into a flat surface, modelled as the basal thrust of the Dalmatian tectonic unit, delineated at the depth of 23 km underneath the basal thrust of the High Karst unit. To the SW from the mainshock hypocentre depth, the geometry of the seismogenic source is delineated by a successive flat and ramp, the latter corresponding to the 53° NE-dipping nodal plane reported by Govorčin et al. (2020) as the seismogenic source of the mainshock of the Ston–Slano 1996 earthquake sequence. Thus, our modelling suggests that both mainshocks, although at the horizontal distance of c. 35 km, could be attributed to the same composite seismogenic source (either to the HRCS004 or HRCS001 sensu Basili et al., 2013; Kastelic et al., 2013, Fig. 2), corresponding to the basal thrust of the Dalmatian tectonic unit, i.e. to the two NE-dipping and blind ramps of this basal thrust.

5. Conclusions

In the southern part of the External Dinarides, in the southeastern part of Bosnia and Herzegovina in the Municipality of Berkovići, an earthquake sequence began on 22 April 2022 with the mainshock of M_L

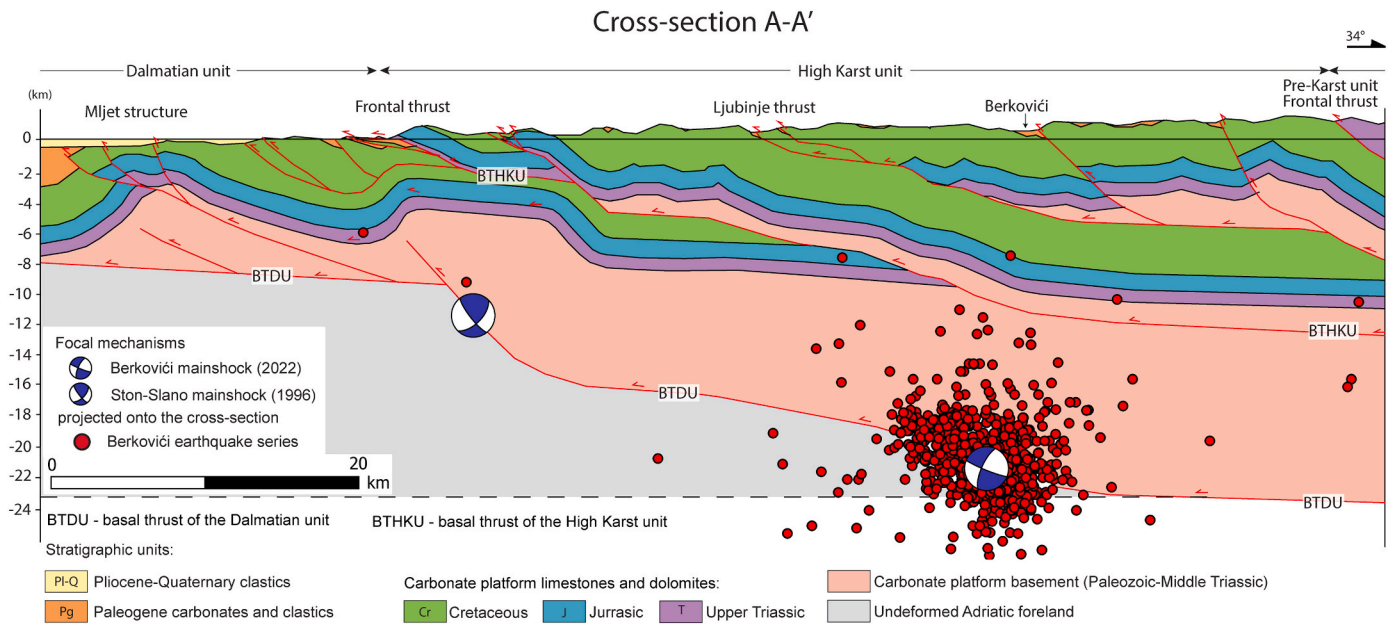

Fig. 12. Preliminary regional geological cross-section across the Berkovići and Ston-Slano epicentral area, SW part of the Dalmatian, High Karst, and Pre-Karst tectonic units, considering only faults with significant displacement. Geological cross-section is constructed based on the Basic Geological Map of SFRY, sheets: Trebinje (Natević and Petrović, 1967), Nevesinje (Mojičević and Laušević, 1969), Dubrovnik (Marković, 1971) and Ston (Raić et al., 1980), supplemented by own field measurements and by interpretation and correlation with 2D reflection seismic cross-sections provided by Croatian Hydrocarbon Agency. For the location of the cross-section see Fig. 2. BTDU – the basal thrust of the Dalmatian tectonic unit, BTHKU – basal thrusts of the High Karst.

= 6.0. Its maximum intensity was estimated as VII EMS for the Municipality of Berkovići where 29% buildings were damaged, mostly of vulnerability class A–B, and many of them were in relatively poor condition prior to the earthquake. This epicentral area is known to have produced only one strong earthquake in the past (in 1927, of maximum intensity VIII MCS in Ljubinje), and this is the first opportunity to study a strong event and its aftershocks there, as recorded by a modern seismic network.

We analysed the first nine months of the sequence, the period between 22 April 2022 and 22 January 2023. The locations were calculated with source-specific station corrections as mean of solutions for 54 combinations of velocity models and program control parameters. The analysis of temporal change of aleatory variation and epistemic uncertainty of locations showed that they strongly depend on the station coverage, especially for the focal depth. The largest influence is imparted by the closest seismic station DF01 (Ljubinje), 15 km to the south of the mainshock epicentre.

The mainshock occurred on 22 April 2022 21:07:48.6 UTC at the depth of 22 km with magnitude $M_L = 6.0$ ($M_W = 5.7$). In total, we located 7217 earthquakes and the sequence's catalogue can be considered complete for magnitude $M_c = 1.3$. Focal depths ranging between 15 and 30 km are larger than average for the whole area of the External Dinarides, but consistent with so far observed depths in the narrow SE–NW striking zone of mid-crustal events that includes the Berkovići epicentral area. Epicentres are mostly concentrated in four earthquake clusters, with the largest one containing aftershocks related to the main seismogenic fault. Combining the information from the cross-sections through the hypocentral volume and epicentral spatial distribution, we propose that the rupture spread from the hypocentre down-dip, i.e. mostly to the north, northeast, and east. Seismicity immediately spread from the mainshock bilaterally further along the strike, to the NW and SE, and to the SW. In later stages, it was mostly concentrated close to the mainshock while slowly decreasing, until December 2022 when it increased, predominantly as a cluster about 6 km north of the mainshock.

Focal mechanisms were determined with the first-motion polarity method for eight earthquakes: five of them, including the mainshock, were due to reverse faulting on faults striking in the Dinaric direction, with the preferred main fault gently dipping to the northeast. However, three earthquakes were due to normal faulting, unexpected for this area. Two of them occurred close to each other, on a fault striking in the SW–NE direction and within the separate aftershock cluster elongated along the strike. It seems plausible that those two aftershocks were caused by Coulomb stress redistribution following the main rupture, which increased stresses and reactivated old normal faults of right orientation (if they exist there). The third normal aftershock occurred 55 h after the mainshock, probably on the same fault, and with almost exactly opposite mechanism. This may be explained by temporary reversal of the stresses after a total stress drop, resulting in a dynamic rupture overshoot due to inertial effects, and later recovery. A prerequisite for it is a compliant fault zone, with reduced rigidity in its neighbourhood compared to the surrounding host rocks – fault zone lithology may play an important role in their formation. If this is the case, it may have implications for seismogenesis and tectonic processes in these parts of External Dinarides.

The modelled geometry of the basal thrusts of the High Karst and the Dalmatian tectonic units along the cross-section from the Adriatic coast towards northeast suggests that both the Ston–Slano event of 1996 and the Berkovići earthquake of 2022, although at the horizontal distance of about 35 km one from another, could be attributed to the same composite seismogenic source. It corresponds to the basal thrust of the Dalmatian tectonic unit, i.e. to the two NE-dipping and blind ramps of this basal thrust.

CRediT authorship contribution statement

Iva Dasović: Writing – original draft, Supervision, Methodology, Investigation, Formal analysis, Conceptualization, Validation, Writing – review & editing. **Marijan Herak:** Writing – original draft, Visualization, Software, Resources, Methodology, Investigation, Formal analysis, Data curation, Conceptualization, Validation, Writing – review & editing. **Davorka Herak:** Writing – original draft, Validation, Investigation, Formal analysis, Data curation. **Helena Latečki:** Writing – original draft, Visualization, Investigation, Formal analysis, Data curation.

Marin Sečanj: Writing – original draft, Visualization, Validation, Methodology, Investigation, Formal analysis, Data curation, Conceptualization, Writing – review & editing. **Bruno Tomljenović:** Writing – original draft, Validation, Supervision, Methodology, Investigation, Formal analysis, Conceptualization, Writing – review & editing. **Snježana Cvijić-Amulić:** Writing – original draft, Validation, Resources, Investigation, Data curation. **Josip Stipčević:** Writing – original draft, Validation, Supervision, Resources, Project administration, Funding acquisition, Formal analysis.

Declaration of competing interest

The authors declare that they have no known competing financial interests or personal relationships that could have appeared to influence the work reported in this paper.

Data availability

The earthquake catalogue for the first nine months of the Berkovići 2022 earthquake sequence is in Supplementary data.

Acknowledgements

The installation of temporary stations DF01, DF02 and DF03 in Bosnia and Herzegovina has only been possible thanks to the collaboration between the Republic Hydrometeorological Service of the Republic of Srpska from Banja Luka (BIH) and the Department of Geophysics, Faculty of Science, University of Zagreb (HR). Croatian Seismological Survey of the Department of Geophysics, Faculty of Science, University of Zagreb made available seismograms from the seismic stations they deployed and maintain, as well as citizens' reports to their online questionnaire which we used in our macroseismic analysis. We are thankful to municipalities of Berkovići, Ljubinje, Stolac, Nevesinje, Trebinje and Bileća for sending us their official reports on damage or other types of data. We also thank the Public Fire Department of Metković for information on damage in Metković. The Croatian Hydrocarbon Agency is greatly acknowledged for making the legacy of reflection seismic profiles available. Modelling in the MOVE 2019.1 structural geology software was possible thanks to an academic licence from Petex to the University of Zagreb.

This study has been partly supported by the Croatian Science Foundation (grant IP2020-02-3960 – the DuFAULT project) and the CRONOS project supported by the Norway Grants (Norwegian Financial Mechanism 2014–2021, grant 04-UBS-U-0002/22-90).

Appendix A. Macroseismic analysis of the Berkovići 2022 mainshock

To estimate macroseismic intensities for the mainshock according to European Macroseismic Scale (EMS, Grünthal, 1998) we used various types of data. Data are gathered from the online questionnaire of the Croatian Seismological Survey, reports received by the **European-Mediterranean Seismological Centre** (EMSC; URL6, 2023), data (photographs, videos, interviews etc.) available on the internet news portals (national, regional, and local), reports from affected municipalities' webpages, as well as official reports and data (photos) from several municipalities and their civil protection organisations affected by earthquake shaking. We also used information on the mainshock effects collected in field by personal reconnaissance of the shaken area. However, these were only of limited extent – mostly in the border area of Croatia and Bosnia and Herzegovina (Slano, Trnova, Trnovica, Lisac, Zavala, Trnčina, Hutovo), as well as Ljubinje and Stolac. Fig. A1 shows the intensity map.

The mainshock epicentral area is a rural, mountainous region of low population density: the Municipalities of Berkovići, Ljubinje and Stolac have population densities of 8.5/km^2 (*URL7*, 2023), 11/km^2 (*URL8*, 2023), and 45/km^2 (*URL9*, 2023), respectively.

The maximum intensity VII EMS was assigned to the Municipality of Berkovići (2114 inhabitants, *URL7*, 2023) in the proximity of the epicentre. It is based on the official report of the Municipality (S1 in the References), and photographs and information obtained on the internet portals. The report states that 29% of the building in the municipality were damaged or destroyed – 12 buildings (two residential buildings, nine stables and an auxiliary building) have been heavily damaged and are designated for demolition. However, in the report damage was categorised differently than in EMS, not taking the vulnerability class into account. By investigating alternative sources (published photographs) and knowing the traditional type of construction, we presume that most of the damaged buildings are of vulnerability classes A and B, and some of vulnerability class C. The total damage was estimated at about 1.25 million EUR.

Fig. A1. Macroseismic intensity (EMS) map for the mainshock of the Berkovići 2022 earthquake series. The dark blue star marks the instrumentally determined epicentre. Intensities are marked in different colours according to legend in the figure. (For interpretation of the references to colour in this figure legend, the reader is referred to the web version of this article.)

Ljubinje is the municipality of 3511 inhabitants whereas the main settlement itself has 2744 inhabitants (*URL*8, 2023). According to the official report of Ljubinje municipality (S2 in the References), damage was found on 231 buildings or facilities (221 residential buildings and 9 public buildings): 78% were categorised equivalently to damage grade 1 and 2, and six buildings and facilities were declared beyond repair – however, they were in poor condition before an earthquake struck. The total damage was estimated at about 1.8 million EUR. We estimate the intensity as VI–VII EMS.

Stolac is the municipality of 14,889 inhabitants, and the town of Stolac has 3816 inhabitants (*URL*9, 2023). The official report mentions 532 damaged buildings (houses, public buildings, stables, and auxiliary facilities): most of the damage is reported as cracked inner walls (possibly only plaster in some cases) and ceilings, displaced roof tiles, light and heavy damage of chimneys. As for Berkovići, we do not have information on buildings' vulnerability class. The total damage is estimated at about 2.3 million EUR. Unfortunately, in Stolac, a 28-year-old woman lost her life to a rockfall caused by an earthquake that hit her house, and ten people were injured. The effects were found to be consistent with the intensity of VI–VII EMS.

Nevesinje is a settlement (5162 inhabitants; *URL*10, 2023) and a municipality (12,961 inhabitants; *URL*10, 2023) north of Berkovići. According to data obtained from the Municipality, the total number of damage reports was 80, but only 40 reports with damage estimate exceeding 50 EUR were taken into account. Mostly vulnerability class A and/or B buildings and/or in poor state were damaged, especially if on soft ground. Damage is dominantly in form of cracks on inner walls and facade, and/or dislocated roof tiles – it can be classified as the 1st and 2nd grade. Some class A buildings also suffered damage to load-bearing walls. Damage in the amount of ≈3400 EUR was determined. The intensity is estimated as V EMS.

The damage was reported within about 40 km from the mainshock epicentre. In Bosnia and Herzegovina, damage of grade 1 or grade 2 is reported in towns and municipalities of Čapljina (VI EMS), Mostar (VI EMS), Nevesinje (V EMS), Bileća (V EMS), and Trebinje (V EMS). In Croatia, damage of grade 1 and/or 2 was observed in Metković (V–VI EMS) and Trnovica (VI EMS). In the area between Vrgorac and the border to Montenegro, intensity V EMS predominates mostly due to the description of how people felt the earthquake (most were awakened, scared and ran outdoors, strong to very strong shaking) and how the shaking affected objects (moving or fallen objects, spilling of fluids, etc.) rather than the damage it caused. The average radius of the intensity IV EMS is found to be about 150 km.

The greater area affected by the earthquake is a karstic area (limestone and dolomites) with rather thin sediments in the valleys or near the rivers. Thus, buildings are mostly built on a hard rock. Soft soil, however, dominates in the Neretva River delta where Metković and Opuzen are situated and where relatively thick sediments can be found, as well as upstream to Čapljina.

Appendix B. Supplementary data

Earthquake catalogue of the Berkovići 2022 sequence for the first nine months (22 Apr 2022–22 Jan 2023) of activity. Supplementary data to this article can be found online at [https://doi.org/10.1016/j.tecto.2024.230253].

References

Albini, P., 2015. The Great 1667 Dalmatia Earthquake, An In-Depth Case Study. Springer International Publishing, p. 147.

Albini, P., Rovida, A., 2016. From written records to seismic parameters: the case of the 6 April 1667 Dalmatia earthquake. Geosci. Lett. 3 (30) https://doi.org/10.1186/s40562-016-0063-2.

Babić, Lj, Zupanič, J., 2008. Evolution of a river-fed foreland basin fill: the North Dalmatian flysch revisited (Eocene, outer Dinarides). Natura Croatica 17 (4), 357–374.

Balling, P., Tomljenović, B., Schmid, S.M., Ustaszewski, K., 2021a. Contrasting along-strike deformational styles in the central external Dinarides assessed by balanced cross-sections: Implications for the tectonic evolution of its Paleogene flexural foreland basin system. Glob. Planet. Chang. 205, 103587 https://doi.org/10.1016/j.gloplacha.2021.10358.

Balling, P., Grützner, C., Tomljenović, B., Spakman, W., Ustaszewski, K., 2021b. Post-collisional mantle delamination in the Dinarides implied from staircases of Oligo-Miocene uplifted marine terraces. Sci. Rep. 11, 2685. https://doi.org/10.1038/s41598-021-81561-5.

Basili, R., Kastelic, V., Demircioglu, M.B., Garcia Moreno, D., Nemser, E.S., Petricca, P., Sboras, S.P., Besana-Ostman, G.M., Cabral, J., Camelbeeck, T., Caputo, R., Danciu, L., Domac, H., Fonseca, J., García-Mayordomo, J., Giardini, D., Glavatovic, B., Gulen, L., Ince, Y., Pavlides, S., Sesetyan, K., Tarabusi, G., Tiberti, M. M., Utkucu, M., Valensise, G., Vanneste, K., Vilanova, S., Wössner, J., 2013. The European Database of Seismogenic Faults (EDSF) Compiled in the Framework of the Project SHARE. https://doi.org/10.6092/INGV.IT-SHARE-EDSF.

Belinić, T., Kolínský, P., Stipčević, J., AlpArray Working Group, 2020. Shear-wave velocity structure beneath the Dinarides from the inversion of Rayleigh-wave dispersion. Earth Planet. Sci. Lett. 555, 116686 https://doi.org/10.1016/j.epsl.2020.116686.

Bennett, R.A., Hreinsdóttir, S., Buble, G., Bašić, T., Bačić, Ž., Marjanović, M., Casale, G., Gendaszek, A., Cowan, D., 2008. Eocene to present subduction of southern Adria mantle lithosphere beneath the Dinarides. Geology 36, 3–6. https://doi.org/10.1130/G24136A.1.

Beroza, G.C., Zoback, M.D., 1993. Mechanism Diversity of the Loma Prieta Aftershocks and the Mechanics of Mainshock-Aftershock Interaction. Science 299, 210–213.

CR: University of Zagreb, 2001. Croatian Seismograph Network. International Federation of Digital Seismograph Networks. https://doi.org/10.7914/SN/CR.

EIDA, 2022–2023. European Integrated Data Archive. http://eida.gfz-potsdam.de/webdc3/. Last accessed on 28 May 2023.

EMODnet Bathymetry Consortium, 2022. EMODnet digital bathymetry (DTM 2022). https://emodnet.ec.europa.eu/geoviewer.

European digital elevation model (EU-DEM), 2016. Copernicus data version 1.1,. https://land.copernicus.eu/imagery-in-situ/eu-dem.

Faivre, S., Bakran-Petricioli, T., Barešić, J., Horvatić, D., 2021a. Lithophyllum rims as biological markers for constraining palaeoseismic events and relative sea-level variations during the last 3.3 ka on Lopud Island, southern Adriatic, Croatia. Glob. Planet. Chang. 202, 103517 https://doi.org/10.1016/j.gloplacha.2021.103517.

Faivre, S., Bakran-Petricioli, T., Herak, M., Barešić, J., Borković, D., 2021b. Late Holocene interplay between coseismic uplift events and interseismic subsidence at Koločep island and Grebeni islets in the Dubrovnik archipelago (southern Adriatic, Croatia). Quat. Sci. Rev. 274, 107284 https://doi.org/10.1016/j.quascirev.2021.107284.

Faivre, S., Bakran-Petricioli, T., Kaniewski, D., Marriner, N., Tomljenović, B., Sečanj, M., Horvatić, D., Barešić, J., Morhange, C., Drysdale, R.N., 2023. Driving processes of relative sea-level change in the Adriatic during the past two millennia: from local tectonic movements in the Dubrovnik archipelago (Jakljan and Šipan islands) to global mean sea level contributions (Central Mediterranean). Glob. Planet. Chang. 227, 104158. https://doi.org/10.1016/j.gloplacha.2023.104158.

GCMT. https://www.globalcmt.org/, 2022. Last accessed on 28 May 2023.

GFZ. https://geofon.gfz-potsdam.de/eqinfo/form.php?lang=en, 2022. Last accessed on 28 May 2023.

Govorčin, M., Herak, M., Matoš, B., Pribičević, B., Vlahović, I., 2020. Constraints on Complex Faulting during the 1996 Ston-Slano (Croatia) Earthquake Inferred from the DInSAR. Seismological and Geological Observations. Remote Sens. 12 (7), 1157. https://doi.org/10.3390/rs12071157.

Grenerczy, G., Sella, G., Stein, S., Kenyeres, A., 2005. Tectonic implications of the GPS velocity field in the northern Adriatic region. Geophys. Res. Lett. 32, L16311. https://doi.org/10.1029/2005GL022947.

Grünthal, G. (Ed.), 1998. European Macroseismic Scale 1998, Cahiers du Centre Europèen de Gèodynamique et de Seismologie, 15. Conseil de l'Europe, Luxembourg, p. 99.

Herak, M., 1989. HYPOSEARCH – an earthquake location program. Comput. Geosci. 15 (7), 1157–1162. https://doi.org/10.1016/0098-3004(89)90127-1.

Herak, M., 2020. Conversion between the local magnitude (ML) and the moment magnitude (Mw) for earthquakes in the Croatian Earthquake Catalogue. Geofizika 37, 197–211. https://doi.org/10.15233/gfz.2020.37.10.

Herak, M., Herak, D., 2023. Properties of the Petrinja (Croatia) earthquake sequence of 2020–2021 – Results of seismological research for the first six months of activity. Tectonophysics 858, 229885. https://doi.org/10.1016/j.tecto.2023.229885.

Herak, M., Herak, D., Markušić, S., 1996. Revision of the earthquake catalogue and seismicity of Croatia. Terra Nova 8, 86–94.

Herak, M., Allegretti, I., Herak, D., Kuk, K., Kuk, V., Marić, K., Markušić, S., Stipčević, J., 2010. HVSR of ambient noise in Ston (Croatia)—Comparison with theoretical spectra and with the damage distribution after the 1996 Ston–Slano earthquake. Bull. Earthq. Eng. 8, 483–499.

Herak, M., Herak, D., Dasović, I., 2016. Fault-plane solutions and stress orientation in the greater region of Northern and Central Dinarides. In: Book of Abstracts, 35th General Assembly of the European Seismological Commission, 5–8 September 2016, Trieste, Italy, ESC2016–480.

Herak, D., Herak, M., Vrkić, I., 2017. Velika trešnja, seizmičnost i potresna opasnost na širem dubrovačkom području. Dubrovnik: časopis za književnost i znanost. XXVIII 1, 5–18 (In Croatian).

Herak, M., Herak, D., Orlić, N., 2021. Properties of the Zagreb 22 March 2020 earthquake sequence – analyses of the full year of aftershock recording. Geofizika 38, 93–116. https://doi.org/10.15233/gfz.2021.38.6.

Herak, D., Herak, M., Vrkić, I., 2023. The Earthquake of 13 April 1850 near Ston. Macroseismic Analyses. Seismol. Res. Lett, Croatia. https://doi.org/10.1785/0220230299.

HU: Kövesligethy Radó Seismological Observatory (Geodetic and Geophysical Institute), 1992. Research Centre for Astronomy and Earth Sciences, Hungarian Academy of Sciences (MTA CSFK GGI KRSZO). In: Hungarian National Seismological Network. GFZ Data Services. 10.14470/UH028726.

Ide, S., Baltay, A., Beroza, G., 2011. Shallow Dynamic Overshoot and Energetic Deep Rupture in the 2011 Mw 9.0 Tohoku-Oki Earthquake. Science 332 (6036), 1426–1429. https://doi.org/10.1126/science.1207020.

INGV. http://rcmt2.bo.ingv.it/, 2022. Last accessed on 28 May 2023.

International Seismological Centre, 2021. ISC-GEM Earthquake Catalogue. https://doi.org/10.31905/D808B825.

IV: Istituto Nazionale di Geofisica e Vulcanologia (INGV), 2005. Rete Sismica Nazionale (RSN). Istituto Nazionale di Geofisica e Vulcanologia (INGV). 10.13127/SD/X0FXnH7QfY.

Kang, J., Duan, B., 2015. Elastic and inelastic responses of compliant fault zones to nearby earthquakes in three dimensions: a parameter-space study. Geophys. J. Int. 201, 1195–1214. https://doi.org/10.1093/gji/ggv075.

Kastelic, V., Carafa, M.M.C., 2012. Fault slip rates for the active External Dinarides thrust-and-fold belt. Tectonics 31, TC3019. https://doi.org/10.1029/2011TC003022.

Kastelic, V., Vannoli, P., Burrato, P., Fracassi, U., Tiberti, M.M., Valensise, G., 2013. Seismogenic sources in the Adriatic Domain. Mar. Pet. Geol. 42, 191–213. https://doi.org/10.1016/j.marpetgeo.2012.08.002.

Kuk, V., Prelogović, E., Dragičević, I., 2000. Seismotectonically active zones in the Dinarides. Geologia Croatica 53 (2), 295–303. https://doi.org/10.4154/GC.2000.06.

Marković, B., 1971. Basic Geological Map of SFRY, M 1:100.000, Dubrovnik Sheet K34-49. Federal Geological Institute Beograd.

Markušić, S., Herak, D., Ivančić, I., Sović, I., Herak, M., Prelogović, E., 1998. Seismicity of Croatia in the period 1993–1996 and the Ston–Slano earthquake of 1996. Geofizika 15, 83–101.

Materna, K., Bürgmann, R., 2016. Contrasts in compliantfault zone properties inferred from geodetic measurements in the San Francisco Bay area. J. Geophys. Res. Solid Earth 121, 6916–6931. https://doi.org/10.1002/2016JB013243.

McGarr, A., 1999. On relating apparent stress to the stress causing earthquake fault slip. J. Geophys. Res. 104 (B2), 3003–3011.

Medvedev, S.V., 1978. Definition of the Intensity of Earthquakes (in Russian). Voprosi Inzhenermoy Seysmologii 19, 108–116.

Medvedev, S., Sponheuer, W., Karník, V., 1964. Neue seismische Skala, In: 7. Tagung der Europäischen Seismologischen Kommission vom 24.9. bis 30.9.1962. in Jena, Veröff. Institut für Bodendynamik und Erdbebenforschung in Jena, Deutsche Akademie der Wissenschaften zu Berlin 77, 69–76.

MN: MedNet Project Partner Institutions, 1990. Mediterranean Very Broadband Seismographic Network (MedNet). Istituto Nazionale di Geofisica e Vulcanologia (INGV). 10.13127/SD/fBBBtDtd6q.

Mojičević, M., Laušević, M., 1969. Basic Geological Map of SFRY, M 1:100.000, Nevesinje Sheet K34–25. Federal Geological Institute Beograd.

Natević, L.J., Petrović, V., 1967. Basic Geological Map of the SFRY, M 1:100.000, Trebinje Sheet K34-37. Federal Geological Institute Beograd.

NI: OGS (Istituto Nazionale di Oceanografia e di Geofisica Sperimentale) and University of Trieste, 2002. North-East Italy Broadband Network. International Federation of Digital Seismograph Networks. https://doi.org/10.7914/SN/NI.

Nie, S., Barbot, S., 2022. Rupture styles linked to recurrence patterns in seismic cycles with a compliant fault zone. Earth Planet. Sci. Lett. 591, 117593 https://doi.org/10.1016/j.epsl.2022.117593.

Nooshiri, N., 2019. SCOTER – Multiple-Earthquake Location by Using Static and Source-Specific Station COrrection TERms, Scientific Technical Report - STR Data, 19/05.

GFZ German Research Centre for Geosciences, Potsdam, p. 31. https://doi.org/10.2312/GFZ.b103-19056.
OCA. http://sismoazur.oca.eu/focal_mechanism_emsc, 2022. Last accessed on 28 May 2023.
OE: ZAMG - Zentralanstalt für Meterologie und Geodynamik, 1987. Austrian Seismic Network. International Federation of Digital Seismograph Networks. https://doi.org/10.7914/SN/OE.
Orlić, N., Herak, M., Miklić, D., 2007–2021. SANDI – Seismogram ANalysis and DIsplay, Computer Program, Department of Geophysics. Faculty of Science, University of Zagreb.
Prtoljan, B., Jamičić, D., Cvetko Tešović, B., Kratković, I., Markulin, Ž., 2007. The influence of late cretaceous synsedimentary deformation on the Cenozoic structuration of the middle Adriatic, Croatia. Geodin. Acta 20 (5), 287–300. https://doi.org/10.3166/ga.20.287-300.
Raić, V., Papeš, J., Behilović, S., Crnolatac, I., Mojićević, M., Ranović, M., Slišković, T., Đorđević, B., Golo, B., Ahac, A., Luburić, P., Marić, L.J., 1975. Basic Geological Map of SFRY, M 1:100.000, Metković Sheet K33-36. Federal Geological Institute Beograd.
Raić, V., Papeš, J., Ahac, A., Korolija, B., Borović, I., Grimani, I., Marinčić, S., 1980. Basic Geological Map of SFRY, M 1:100.000, Ston Sheet K33-48. Federal Geological Institute Beograd.
Ratchkovski, N.A., 2017. Change in stress directions along the central Denali fault, Alaska after the 2002 earthquake sequence. Geophys. Res. Lett. 30 (19) https://doi.org/10.1029/2003GL017905.
Richards-Dinger, K.B., Shearer, P.M., 2000. Earthquake locations in southern California obtained using source-specific station terms. J. Geophys. Res. 105, 10939–10960. https://doi.org/10.1029/2000JB900014.
S1: Republika Srpska, Opština Berkovići, 2022. Elaborat o procjenjenim štetama od zemljotresa u Opštini Berkovići 2022. Godine, Berkovići, June 2022, 8 pp. *(In Serbian.)*.
S2: Republika Srpska, Opština Ljubinje, 2022. Elaborat o procjenjenim štetama od zemljotresa u Opštini Ljubinje 2022. godine, Ljubinje, August 2022, 8 pp. *(In Serbian.)*.
Sattari, A., 2018. Finite Element Modelling of Induced Rupture on Faults with Non-negligible Cohesion. Doctoral thesis,. University of Calgary, Calgary, Canada. https://doi.org/10.11575/PRISM/32904.
Schmid, S.M., Fügenschuh, B., Kounov, A., Matenco, L., Nievergelt, P., Oberhänsli, R., Pleuger, J., Schefer, S., Schuster, R., Tomljenović, B., Ustaszewski, K., van Hinsbergen, D.J.J., 2020. Tectonic units of the Alpine collision zone between Eastern Alps and western Turkey. Gondwana Res. 78, 308–374. https://doi.org/10.1016/j.gr.2019.07.005.
Schmitz, B., Biermanns, P., Hinsch, R., Đaković, M., Onuzi, K., Reicherter, K., Ustaszewski, K., 2020. Ongoing shortening in the Dinarides fold-and-thrust belt: a new structural model of the 1979 (Mw 7.1) Montenegro earthquake epicentral region. J. Struct. Geol. 141, 104192 https://doi.org/10.1016/j.jsg.2020.104192.
SJ: Seismological Survey of Serbia, 1906. Serbian Seismological Network. International Federation of Digital Seismograph Networks. https://doi.org/10.7914/SN/SJ.
SL: Slovenian Environment Agency, 1990. Seismic Network of the Republic of Slovenia. International Federation of Digital Seismograph Networks. https://doi.org/10.7914/SN/SL.
Toda, S., Stein, R.S., Sevilgen, V., Lin, J., 2011. Coulomb 3.3 Graphic-rich deformation and stress-change software for earthquake, tectonic, and volcano research and teaching—user guide. In: U.S. Geological Survey Open-File Report 2011–1060, p. 63.
URL1. https://twitter.com/SimoneAtzori73/status/1520389729090473984?s=20, 2023. Last accessed on 28 May.
URL10. https://en.wikipedia.org/wiki/Nevesinje, 2023. Last accessed on 28 May.
URL2. https://edsf13.ingv.it/SHARE_WP3.2_Database.html, 2023. Last accessed on 28 May.
URL3. https://projectdufault.geof.pmf.unizg.hr/, 2023. Last accessed on 28 May.
URL4. https://orfeus.readthedocs.io/en/latest/adria_array_main.html, 2023. Last accessed on 28 May.
URL5. https://projekt-cronos.hr/en/home/, 2023. Last accessed on 28 May.
URL6, 2023. https://www.emsc-csem.org/Earthquake/earthquake.php?id=1121117. Last accessed on 28 May.
URL7. https://en.wikipedia.org/wiki/Berkovi%C4%87i, 2023. Last accessed on 28 May.
URL8. https://en.wikipedia.org/wiki/Ljubinje, 2023. Last accessed on 28 May.
URL9. https://en.wikipedia.org/wiki/Stolac, 2023. Last accessed on 28 May.
USGS. https://earthquake.usgs.gov/earthquakes/eventpage/us6000hfqj/moment-tensor, 2022. Last accessed on 28 May 2023.
Utsu, T., 1961. A statistical study on the occurrence of aftershocks. Geophys. Mag. 30, 521–605.
van Unen, M., Matenco, L., Nader, F.H., Darnault, R., Mandic, O., Demir, V., 2019a. Kinematics of Foreland-Vergent Crustal Accretion: Inferences from the Dinarides Evolution. Tectonics 38, 49–76. https://doi.org/10.1029/2018TC005066.
van Unen, M., Matenco, L., Demir, V., Nader, F.H., Darnault, R., Mandic, O., 2019b. Transfer of deformation during indentation: Inferences from the post-middle Miocene evolution of the Dinarides. Glob. Planet. Chang. 182, 103027 https://doi.org/10.1016/j.gloplacha.2019.103027.
Vlahović, I., Tišljar, J., Velić, I., Matičec, D., 2005. Evolution of the Adriatic Carbonate Platform: Palaeogeography, main events and depositional dynamics. Palaeogeogr. Palaeoclimatol. Palaeoecol. 220, 333–360. https://doi.org/10.1016/j.palaeo.2005.01.011.
Vlahović, I., Mandic, O., Mrinjek, E., Bergant, S., Ćosović, V., de Leeuw, A., Enos, P., Hrvatović, H., Matičec, D., Mikša, G., Nemec, W., Pavelić, D., Pencinger, V., Velić, I., Vranjković, A., 2012. Marine to continental depositional systems of Outer Dinarides foreland and intra-montane basins (Eocene-Miocene, Croatia and Bosnia and Herzegovina). J. Alpine Geol. 54, 405–470.
Weber, J., Vrabec, M., Pavlovčič-Prešeren, P., Dixon, T., Jiang, Y., Stopar, B., 2010. GPS-derived motion of the Adriatic microplate from Istria Peninsula and Po Plain sites, and geodynamic implications. Tectonophysics 483, 214–222. https://doi.org/10.1016/j.tecto.2009.09.001.
Wells, D.L., Coppersmith, K.J., 1994. New Empirical Relationships among Magnitude, Rupture Length, Rupture Width, Rupture Area, and Surface Displacement. Bull. Seismol. Soc. Am. 84 (4), 974–1002. https://doi.org/10.1785/BSSA0840040974.
WS: Seismic Network of Republika Srpska, 2011. Republicki Hidrometeorološki Zavod. International Federation of Digital Seismograph Networks. https://www.fdsn.org/networks/detail/WS/. https://rhmzrs.com/seizmologija/seizmoloska-mreza/.
Z3: AlpArray Seismic Network, 2015. AlpArray Seismic Network (AASN) temporary component. AlpArray Working Group. 10.12686/alparray/z3_2015.

Update

Tectonophysics
Volume 885, Issue , 22 August 2024, Page

DOI: https://doi.org/10.1016/j.tecto.2024.230437

Tectonophysics 885 (2024) 230437

Contents lists available at ScienceDirect

Tectonophysics

journal homepage: www.elsevier.com/locate/tecto

Corrigendum to "The Berkovići (BIH) ML = 6.0 earthquake sequence of 22 April 2022 – seismological and seismotectonic analyses" [Tectonophysics 875 (2024) 230253]

Iva Dasović [a,*], Marijan Herak [a], Davorka Herak [a,1], Helena Latečki [a], Marin Sečanj [a], Bruno Tomljenović [b], Snježana Cvijić-Amulić [c], Josip Stipčević [a]

[a] Department of Geophysics, Faculty of Science, University of Zagreb, Horvatovac 95, 10000 Zagreb, Croatia
[b] Faculty of Mining, Geology and Petroleum Engineering, University of Zagreb, Pierottijeva 6, 10000 Zagreb, Croatia
[c] Republic Hydrometeorological Institute of Republic of Srpska, Put Banja Luka odreda bb, 78000 Banja Luka, P.O. Box: 147, Bosnia and Herzegovina

The authors regret that in the *References* the following reference is missing:

Y5: Obermann, A., Jozinović, D., Cvijic, S., Krehić, A., & Swiss Seismological Service (SED) at ETH Zurich. (2022). Swiss Contribution to AdriaArray Temporary Network. ETH Zurich. https://doi.org/10.12686/SED/NETWORKS/Y5.

Furthermore, In the *Acknowledgments*, the following sentence should be added after the first one: "The Swiss Seismological Service (SED) at ETH Zürich, in collaboration with the Republic Hydrometeorological Service of the Republic of Srpska from Banja Luka and the Hydrometeorological Institute of Federation of Bosnia and Herzegovina from Sarajevo, deployed temporary seismic network Y5 in Bosnia and Herzegovina within the AdriaArray initiative – we acknowledge their efforts, as well as the efforts of the AdriaArray Seismology Group (URL4, 2023)."

The authors would like to apologise for any inconvenience caused.

References

Y5: Obermann, A., Jozinović, D., Cvijic, S., Krehić, A., & Swiss Seismological Service (SED) at ETH Zurich. (2022). Swiss Contribution to AdriaArray Temporary Network. ETH Zurich. https://doi.org/10.12686/SED/NETWORKS/Y5.

URL4: https://orfeus.readthedocs.io/en/latest/adria_array_main.html (Last accessed on 28 May 2023.)

DOI of original article: https://doi.org/10.1016/j.tecto.2024.230253.

* Corresponding author at: Department of Geophysics, Faculty of Science, University of Zagreb, Horvatovac 95, 10000 Zagreb, Croatia.
E-mail address: iva.dasovic@gfz.hr (I. Dasović).
[1] Retired.

https://doi.org/10.1016/j.tecto.2024.230437

Available online 1 August 2024